IEEE Access
Multidisciplinary | Rapid Review | Open Access Journal

Received July 22, 2018, accepted August 21, 2018, date of publication August 27, 2018, date of current version September 21, 2018.

Digital Object Identifier 10.1109/ACCESS.2018.2867214

Switching Techniques and Intelligent Controllers for Induction Motor Drive: Issues and Recommendations

MAHAMMAD A. HANNAN[1], (Senior Member, IEEE), JAMAL ABD ALI[2], PIN JERN KER[1], AZAH MOHAMED[3], (Senior Member, IEEE), MOLLA S. H. LIPU[3], (Student Member, IEEE), AND AINI HUSSAIN[3], (Member, IEEE)

[1]College of Engineering, Institute of Power Engineering, Universiti Tenaga Nasional, Kajang 43000, Malaysia
[2]General Company of Electricity Production Middle Region, Ministry of Electricity, Baghdad 10001, Iraq
[3]Center for Integrated Systems Engineering and Advanced Technologies (INTEGRA), Faculty of Engineering and Built Environment, Universiti Kebangsaan Malaysia, Bangi 43600, Malaysia

Corresponding author: Mahammad A. Hannan (hannan@uniten.edu.my)

This work was supported by the Universiti Tenaga Nasional under Bold 2025 and Grant UNITEN/AVC(R)/RJO10289176/D/1/2018/J49.

ABSTRACT Induction motor drive is widely used in many load applications in approximately 60% of the total industrial load. However, the dynamic configuration of the induction motor, especially a three-phase induction motor (TIM) is a nonlinear system which is not easy to explain theoretically due to sudden changes in load or speed. Therefore, the development of variable speed drive with a robust switching technique and controller design is compulsory for improving the performance efficiency of the TIM. An advanced switching strategy is used for controlling voltage, frequency, and reducing harmonic output signals while an efficient controller is required to regulate currents, speed, torque, and rotor flux. Nevertheless, the development of such controllers and switching methods need the extensive mathematical model and complex online computation. This paper presents a critical review of the different switching techniques, switching pattern of voltage space vectors and switching time to solve the existing problems and enhance the performance of the TIM. Also, the paper describes the different intelligent controller techniques in terms of scalar control and vector control. Consequently, a comprehensive review on conventional controllers such as proportional integral derivative and artificial intelligence controllers such as an artificial neural network, adaptive neural fuzzy inference system, and fuzzy logic control are explained on their structure, algorithm, and mathematical model. Furthermore, the different integrated circuits of the TIM drive controller are reviewed along with benefits and limitations, current issues and challenges, and conclude with recommendations. All the highlighted insights of this review will hopefully lead to increased efforts toward the development of the advanced switching techniques and controllers for the future induction motor drive.

INDEX TERMS Induction motor drive, intelligent controllers, artificial intelligence, switching techniques, SPWM, SVPWM.

I. INTRODUCTION

Globally, the usage of the electric motor as the driving component has been increasing gradually which consumes 40–50% of the total consumption of electricity [1]. TIM accounts for 70% of the electricity consumption for running the industrial loads [2]. The sales of electric motors have increased to 85% due to its attractive features such as low price, simple construction, high reliability and easy maintenance [3]–[5]. Although Direct current (DC) motors are extensively used in areas requiring variable speed operations due to their ease of operation in controlling field flux and torque with field and armature current, they have the disadvantage due to the presence of commutator and brushes, which leads to corrosion and the resulting need for periodic maintenance [6]. Induction motors do not have DC motor problems because of their ruggedness, robustness, efficiency, affordability, ability to withstand harsh or hazardous operating environments, and high output power [7].

The Performance of TIM is significantly affected by the sudden change in load which consumes a lot of

electricity and results in high energy cost [8]. VSD could be used to control the speed and maintain high efficiency [9]. However, obtaining high efficiency and performance for TIMs are greatly dependent on the type of switching technique and controller used in VSD [10], [11]. Pulse width modulation (PWM) switching techniques are generally used to control the switches of voltage source inverters (VSIs) and thereby regulate the output voltage and frequency of TIMs [12]. PWM switching techniques include the sinusoidal PWM (SPWM), hysteresis band PWM (HBPWM), and random pulse width modulation (RPWM). These switching techniques are achieving satisfactory performance. However, in some cases, high computational time, harmonic distortion and switching loss create problems in TIM control. The space vector pulse width modulation (SVPWM) switching technique is one of the best methods for Voltage source inverter (VSI) because of its lower switching losses and ability to minimize the harmonic output signals produced by inverter [5], [13]. However, the SVPWM requires complex online computation, which hinders its real-time implementation. This shortcoming is addressed with an ANN based SVPWM [14]–[16] and ANFIS based SVPWM, which are used for efficient inverter operations [14]. However, the above-mentioned methods require voluminous data and long periods for training and learning the linear and non-linear functions for real-time implementation. A new soft computing method is known as the random forest (RF) regression approach has been used in many applications [17]–[19].

An induction motor consists of controllable semiconductor devices, such as an insulated gate bipolar transistor (IGBT) and metal oxide semiconductor field-effect transistor (MOSFET), which can control motor parameters at the device level [7]. Additionally, an induction motor controller design can be integrated into digital signal processor (DSP), microcontrollers, and field programmable gate array (FPGA) to solve the difficult and fundamental challenge of motor control [20]. Over the years, conventional controller schemes, such as proportional-integral derivative (PID), proportional-integral (PI) controller, and proportional-derivative (PD) controllers, have been used to control TIM drives. The main variables, such as voltages, currents, flux, torque, and speed can be regulated by using the conventional controllers. Hence, conventional controllers are extensively used in several applications of scalar and vector controllers [21]. The researches have also been performed on developing artificial intelligent (AI) controller including ANN, ANFIS, and FLC. However, AI controllers have complex computation and require either trial and error or heuristic procedures, which consumes a lot of time [21]–[23].

In general, the hardware implementation of the TIM drive controller has been many concerns for the proper functioning of the control system. Out of many integrated circuits including dSPACE, Field programmable gate array (FPGA), and Digital signal processor (DSP) have been widely used as controller platforms [7], [20], [24]. However, dSPACE, FPGA are not used in common due to their high cost and lack of capability in operating standalone mode. In contrast, DSP has achieved huge attention and already been employed in many applications because of quick response, embedded processor and requires less power.

This paper deals with a detailed review on switching strategies and intelligent controllers to enhance the future research and development for TIM. The conventional and intelligent control systems, controller techniques with their design and comparison have been discussed in detail. Moreover, various switching techniques including switching pattern, switching time calculation have been highlighted. In addition, the paper addresses the advantages and challenges of various integrated circuits for developing hardware of control system. More importantly, a brief discussion on current issues and challenges on controller design and switching techniques have been demonstrated with some recommendations in order to figure out the future efficient switching techniques and controllers.

II. OVERVIEW OF INDUCTION MOTOR DRIVE

The squirrel-cage TIM is a type of asynchronous AC motor with operating principles based on electromagnetic induction. The main function of the TIM is to transform electrical energy to mechanical energy. The TIM consists of two parts, namely, a stator and a rotor, which are separated by a small air gap. The squirrel-cage TIM is the most widely used because of its insulated winding in the stator and rotor, which are made of solid and cast bars with high conductivity as shown in Fig. 1 [25]–[28].

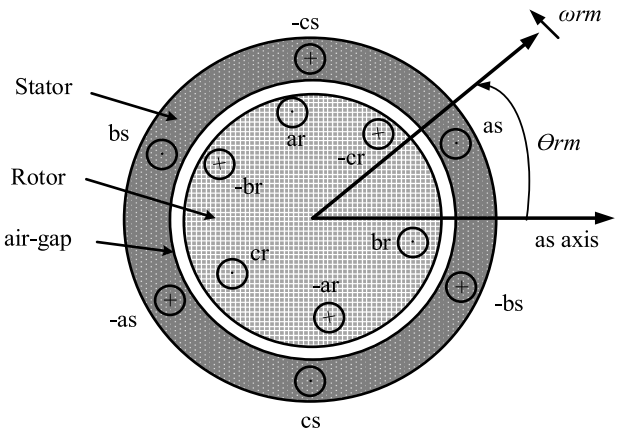

FIGURE 1. Cross Sectional Model of TIM.

The operating principle of TIM starts with supplying three phase voltages to stator winding which makes the rotor run at synchronous speed($\omega_{sm} rad/sec$) ($\omega_s = 2\pi f$ rad/sec), where f is the synchronous frequency. The stator currents generate a rotating magnetic field in the magnetic circuit, which is the stator and rotor cores by the air gap between them. The mechanical synchronous speed ($\omega_{sm} rad/sec$) or($N_{sm} rpm$) depends on the number of poles (P). The synchronous speed

is calculated as follows [29].

$$\omega_{sm} = \frac{2\omega_s}{P} \tag{1}$$

$$N_{sm} = \frac{120f}{P} \tag{2}$$

A. INDUCTION MOTOR MODELING

The mathematical model of the TIM and its drive system are modeled in the computer to present the physical systems [4]. This modelling of the TIM highlights the control parameters of the models. The voltage equations of the magnetic connection between the stator and the rotor circuit for the TIM can be written as follows [30].

$$v_{as} = i_{as}r_s + \frac{d\lambda_{as}}{dt}; \quad v_{bs} = i_{bs}r_s + \frac{d\lambda_{bs}}{dt};$$
$$v_{cs} = i_{cs}r_s + \frac{d\lambda_{cs}}{dt} \tag{3}$$

$$v_{ar} = i_{ar}r_r + \frac{d\lambda_{ar}}{dt}; \quad v_{br} = i_{br}r_r + \frac{d\lambda_{br}}{dt};$$
$$v_{cr} = i_{cr}r_r + \frac{d\lambda_{cr}}{dt} \tag{4}$$

where v_{as}, v_{bs}, v_{cs} are the three-phase stator voltages; v_{ar}, v_{br}, v_{cr} are the three-phase rotor voltages; i_{as}, i_{bs}, i_{cs} are the three-phase stator currents; i_{ar}, i_{br}, i_{cr} are the three-phase rotor currents; r_s is the stator resistance; r_r is the rotor resistance; λ_{as}, λ_{bs}, λ_{cs} are the flux linkages of the stator; and λ_{ar}, λ_{br}, λ_{cr} are the flux linkages of the rotor.

The flux linkages represent the matrix, which is generated between the stator and the rotor windings, in terms of the winding currents and inductances, as shown in the following matrix [25].

$$\begin{bmatrix} \lambda_s^{abc} \\ \lambda_r^{abc} \end{bmatrix} = \begin{bmatrix} L_{ss}^{abc} & L_{sr}^{abc} \\ L_{rs}^{abc} & L_{rr}^{abc} \end{bmatrix} \begin{bmatrix} i_s^{abc} \\ i_r^{abc} \end{bmatrix} \tag{5}$$

where $\boldsymbol{\lambda_s^{abc}} = \begin{bmatrix} \lambda_{as} & \lambda_{bs} & \lambda_{cs} \end{bmatrix}^T$, $\boldsymbol{i_s^{abc}} = \begin{bmatrix} i_{as} & i_{bs} & i_{cs} \end{bmatrix}^T$, $\boldsymbol{\lambda_s^{abc}} = \begin{bmatrix} \lambda_{ar} & \lambda_{br} & \lambda_{cr} \end{bmatrix}^T$, $\boldsymbol{i_r^{abc}} = \begin{bmatrix} i_{ar} & i_{br} & i_{cr} \end{bmatrix}^T$ and superscript T indicates the transpose of the array. The $\boldsymbol{L_{ss}^{abc}}$ matrix represents the stator-to-stator winding inductance, $\boldsymbol{L_{rr}^{abc}}$ denotes the rotor-to-rotor winding inductance, and $\boldsymbol{L_{sr}^{abc}}$ denotes the stator-to-rotor mutual inductance dependent on the rotor angle θ_r as shown in the following matrix [29].

The modern research represents the steady state and transient performance of TIMs with a direct-quadrature-zero (dq0) stationary motor model for solving and facilitating the computation of the TIM performance [3], [7], [28], [31], [32] In this research, a dq0 stationary reference frame is used to develop the simulation model of the motor because of its capability in representing the real-time motor model. Fig. 2 shows the relationship between the abc stator and the rotor dq0 axes. ω_{rm} is the mechanical rotor speed, ω is the dq reference frame speed with the direction of the rotor rotation. Two analysis methods are used for the abc to dq0 transformation, namely, the stationary and synchronously rotating frames. The stationary rotating frame is similar to those normally used for the

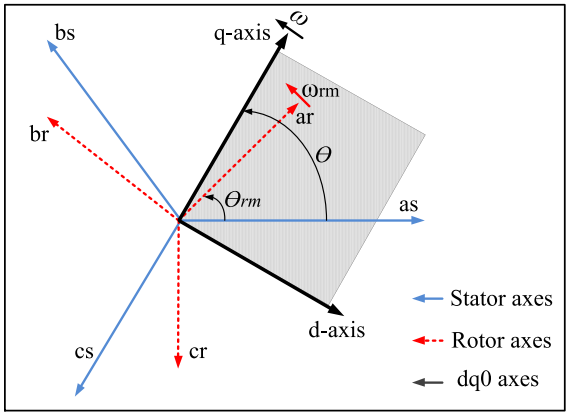

FIGURE 2. Relationship between the abc and dq0 axes.

supply network; in which the speed frame makes$\omega = 0$. The synchronously rotating frame rotates in the same direction as the rotor rotation in which the speed frame becomes $\omega = \omega_s$. The transformation from the abc to the dq0 reference frame and their inverse are given in the following matrix [29], [31], [33].

$$\begin{bmatrix} x_d \\ x_q \\ x_0 \end{bmatrix} = \frac{2}{3} \begin{bmatrix} \cos(\theta) & \cos\left(\theta - \frac{2\pi}{3}\right) & \cos\left(\theta + \frac{2\pi}{3}\right) \\ \sin(\theta) & \sin\left(\theta - \frac{2\pi}{3}\right) & \sin\left(\theta + \frac{2\pi}{3}\right) \\ \frac{1}{2} & \frac{1}{2} & \frac{1}{2} \end{bmatrix} \begin{bmatrix} x_a \\ x_b \\ x_c \end{bmatrix}$$
$$= \left[\boldsymbol{X}_{dq0}(\theta)\right] \begin{bmatrix} x_a \\ x_b \\ x_c \end{bmatrix} \tag{6}$$

$$\begin{bmatrix} x_a \\ x_b \\ x_c \end{bmatrix} = \begin{bmatrix} \cos(\theta) & \sin(\theta) & 1 \\ \cos\left(\theta - \frac{2\pi}{3}\right) & \sin\left(\theta - \frac{2\pi}{3}\right) & 1 \\ \cos\left(\theta + \frac{2\pi}{3}\right) & \sin\left(\theta + \frac{2\pi}{3}\right) & 1 \end{bmatrix} \begin{bmatrix} x_d \\ x_q \\ x_0 \end{bmatrix}$$
$$= \left[\boldsymbol{X}_{dq0}(\theta)\right]^{-1} \begin{bmatrix} x_d \\ x_q \\ x_0 \end{bmatrix} \tag{7}$$

where variable x is the phase voltage, phase current, or phase flux linkage of the TIM.

The stator voltages are transformed to the dq0 voltages into a matrix form, which includes the voltages, currents, and flux linkages to the dq0 reference frame, to obtain the final equation for the dq0 voltages [34].

$$\begin{bmatrix} v_{ds} \\ v_{qs} \\ v_{0s} \end{bmatrix} = \frac{d\theta}{dt} \begin{bmatrix} 0 & 1 & 0 \\ -1 & 0 & 0 \\ 0 & 0 & 0 \end{bmatrix} \begin{bmatrix} \lambda_{ds} \\ \lambda_{qs} \\ \lambda_{0s} \end{bmatrix}$$
$$+ \frac{d}{dt} \begin{bmatrix} \lambda_{ds} \\ \lambda_{qs} \\ \lambda_{0s} \end{bmatrix} + r_s \begin{bmatrix} 1 & 0 & 0 \\ 0 & 1 & 0 \\ 0 & 0 & 1 \end{bmatrix} \begin{bmatrix} i_{ds} \\ i_{qs} \\ i_{0s} \end{bmatrix} \tag{8}$$

Similarly, the rotor voltages are transformed to the dq0 frame into a matrix form which has to be integrated with the mechanical rotor angle $(\theta - \theta_{rm})$ when transferring the voltages, currents, and flux linkages to become $\left[\boldsymbol{X}_{dq0}\,(\theta - \theta_{rm})\right]$ and thereby obtain the following final equations [35].

$$\begin{bmatrix} v_{dr} \\ v_{qr} \\ v_{0r} \end{bmatrix} = \frac{d\,(\theta - \theta_{rm})}{dt} \begin{bmatrix} 0 & 1 & 0 \\ -1 & 0 & 0 \\ 0 & 0 & 0 \end{bmatrix} \begin{bmatrix} \lambda_{dr} \\ \lambda_{qr} \\ \lambda_{0r} \end{bmatrix} + \frac{d}{dt} \begin{bmatrix} \lambda_{dr} \\ \lambda_{qr} \\ \lambda_{0r} \end{bmatrix} + r_r \begin{bmatrix} 1 & 0 & 0 \\ 0 & 1 & 0 \\ 0 & 0 & 1 \end{bmatrix} \begin{bmatrix} i_{dr} \\ i_{qr} \\ i_{0r} \end{bmatrix} \tag{9}$$

The stator dq0 flux linkages are obtained by transforming the stator abc flux linkage, can be expressed [29]:

$$\begin{bmatrix} \lambda_{ds} \\ \lambda_{qs} \\ \lambda_{0s} \end{bmatrix} = \begin{bmatrix} L_{ls} + \frac{3}{2}L_{ss} & 0 & 0 \\ 0 & L_{ls} + \frac{3}{2}L_{ss} & 0 \\ 0 & 0 & L_{ls} \end{bmatrix} \begin{bmatrix} i_{ds} \\ i_{qs} \\ i_{0s} \end{bmatrix} + \begin{bmatrix} \frac{3}{2}L_{sr} & 0 & 0 \\ 0 & \frac{3}{2}L_{sr} & 0 \\ 0 & 0 & 0 \end{bmatrix} \begin{bmatrix} i_{dr} \\ i_{qr} \\ i_{0r} \end{bmatrix} \tag{10}$$

Similarly, the rotor dq0 flux linkages are created through the rotor abc flux linkage

$$\begin{bmatrix} \lambda_{dr} \\ \lambda_{qr} \\ \lambda_{0r} \end{bmatrix} = \begin{bmatrix} \frac{3}{2}L_{sr} & 0 & 0 \\ 0 & \frac{3}{2}L_{sr} & 0 \\ 0 & 0 & 0 \end{bmatrix} \begin{bmatrix} i_{ds} \\ i_{qs} \\ i_{0s} \end{bmatrix} + \begin{bmatrix} L_{lr} + \frac{3}{2}L_{rr} & 0 & 0 \\ 0 & L_{lr} + \frac{3}{2}L_{rr} & 0 \\ 0 & 0 & L_{lr} \end{bmatrix} \begin{bmatrix} i_{dr} \\ i_{qr} \\ i_{0r} \end{bmatrix} \tag{11}$$

On the basis of Eq. (10) and (11), the stator and rotor dq0 flux linkage relationships can be expressed as follows [31], (12), as shown at the bottom of this page, where λ'_{dr}, λ'_{qr} are the referred values in the stator side of the dq rotor flux linkages. i'_{dr}, i'_{qr} are the referred values in the stator side of the dq rotor currents.

The final dq0 reference frame equations are converted to the flux linkage using the formula $\psi = \omega_s\lambda$ and the inductance is also converted into reactance using the formula $x = \omega_s L$ to obtain the following equations [33]:

$$v_{ds} = \frac{1}{\omega_s}\frac{d\psi_{ds}}{dt} + \frac{\omega}{\omega_s}\psi_{qs} + r_s i_{ds} \tag{13}$$

$$v_{qs} = \frac{1}{\omega_s}\frac{d\psi_{qs}}{dt} + \frac{\omega}{\omega_s}\psi_{ds} + r_s i_{qs} \tag{14}$$

$$v_{0s} = \frac{1}{\omega_s}\frac{d\psi_{0s}}{dt} + r_s i_{0s} \tag{15}$$

$$v'_{dr} = \frac{1}{\omega_s}\frac{d\psi'_{dr}}{dt} + \left(\frac{\omega - \omega_{rm}}{\omega_s}\right)\psi'_{qr} + r'_r i'_{dr} \tag{16}$$

$$v'_{qr} = \frac{1}{\omega_s}\frac{d\psi'_{qr}}{dt} - \left(\frac{\omega - \omega_{rm}}{\omega_s}\right)\psi'_{dr} + r'_r i'_{qr} \tag{17}$$

$$v'_{0r} = \frac{1}{\omega_s}\frac{d\psi'_{0r}}{dt} + r'_r i'_{0r} \tag{18}$$

$$\begin{bmatrix} \psi_{ds} \\ \psi_{qs} \\ \psi_{0s} \\ \psi'_{dr} \\ \psi'_{qr} \\ \psi'_{0r} \end{bmatrix} = \begin{bmatrix} x_{ls} + x_m & 0 & 0 & x_m & 0 & 0 \\ 0 & x_{ls} + x_m & 0 & 0 & x_m & 0 \\ 0 & 0 & x_{ls} & 0 & 0 & 0 \\ x_m & 0 & 0 & x'_{lr} + x_m & 0 & 0 \\ 0 & x_m & 0 & 0 & x'_{lr} + x_m & 0 \\ 0 & 0 & 0 & 0 & 0 & x'_{lr} \end{bmatrix} \times \begin{bmatrix} i_{ds} \\ i_{qs} \\ i_{0s} \\ i'_{dr} \\ i'_{qr} \\ i'_{0r} \end{bmatrix} \tag{19}$$

The electromagnetic torque can be present in the following form

$$T_{em} = \frac{3}{2}\frac{P}{2\omega_s}\left(\psi'_{dr}i'_{qr} - \psi'_{qr}i'_{dr}\right) = \frac{3}{2}\frac{P}{2\omega_s}\left(\psi_{qs}i_{ds} - \psi_{ds}i_{qs}\right) = \frac{3}{2}\frac{P}{2\omega_s}x_m\left(i'_{qr}i_{ds} - i'_{dr}i_{qs}\right) \tag{20}$$

The equivalent circuits of the dq0 stationary reference frames are designed by substituting Eq. (19) into Eq. (13) to (18), as shown in Fig. 3.

III. SWITCHING TECHNIQUES

The power semiconductor called the thyristor (silicon controlled rectifier) was invented in the late 1950s. Subsequently, other types of devices, such as triacs, gate turn-off thyristors (GTOs), bipolar power transistors (BPTs), MOSFETs, and IGBTs were manufactured. These power electronic devices ushered a new era for designing power converter circuits, such as AC-DC, DC-DC, AC-DC and

$$\begin{bmatrix} \lambda_{ds} \\ \lambda_{qs} \\ \lambda_{0s} \\ \lambda'_{dr} \\ \lambda'_{qr} \\ \lambda'_{0r} \end{bmatrix} = \begin{bmatrix} L_{ls} + L_m & 0 & 0 & L_m & 0 & 0 \\ 0 & L_{ls} + L_m & 0 & 0 & L_m & 0 \\ 0 & 0 & L_{ls} & 0 & 0 & 0 \\ L_m & 0 & 0 & L'_{lr} + L_m & 0 & 0 \\ 0 & L_m & 0 & 0 & L'_{lr} + L_m & 0 \\ 0 & 0 & 0 & 0 & 0 & L'_{lr} \end{bmatrix} \begin{bmatrix} i_{ds} \\ i_{qs} \\ i_{0s} \\ i'_{dr} \\ i'_{qr} \\ i'_{0r} \end{bmatrix} \tag{12}$$

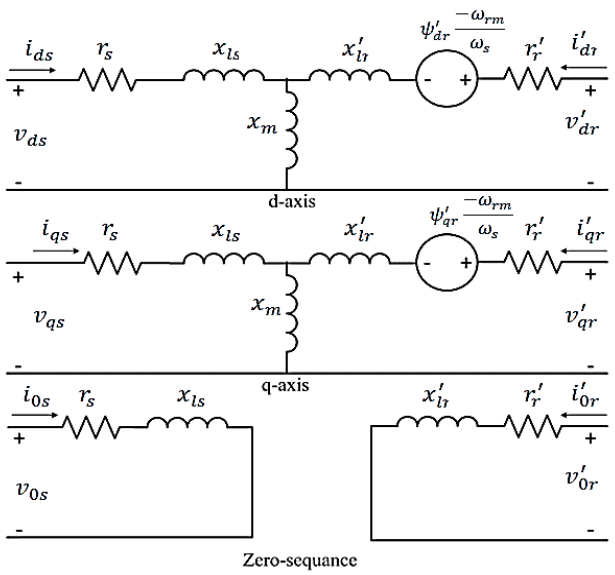

FIGURE 3. Equivalent circuits of the dq0 stationary reference frames of the TIM.

DC-AC converters, which are utilized in many applications [36]. DC power can be converted into AC power at the desired output by a power converter circuit called an inverter. The inverter generates an AC voltage with controlled magnitude and frequency. An inverter can be employed in various applications, including in high voltage DC transmission lines, uninterrupted power supplies, and AC power generation from a fuel cell or photovoltaic (PV) array. An inverter also plays a very important role in the control systems for TIM drives [25], [37]

The inverters can be classified on the basis of the DC voltage and current input source, such as the VSI and current source inverter (CSI). The CSI is normally used for very high power AC motor drive applications. Due to their high switching frequency, VSIs have been used for running the industrial load. Many power electronic devices have been used as switching devices. However, most switching drives are based on IGBTs due to their quick switching, easy control process and high efficiency [29].

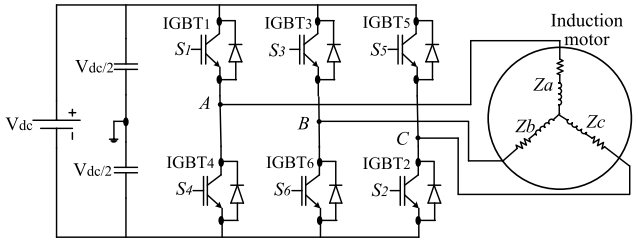

FIGURE 4. Three-phase voltage source inverter with TIM.

A typical VSI comprises of six IGBTs switches as shown in Fig. 4. Each switch has a freewheeling diode that protects the device from reverse voltage when the switch is turned off. The six switches are divided into two groups; the positive group comprising upper switches S_1, S_3, and S_5 and the negative group comprising switches S_4, S_6, and S_2. Each phase is connected in parallel with a pair of switches to the DC source. Two series capacitors are placed on the DC source terminal to smoothen the supply voltages. The controlled power flows to the load when the switches are turned on and off. This tuning is created through the gates of the IGBTs, which are received from the PWM switching signals associated with the control system. Pulse width modulation (PWM) switching techniques are generally used to control the switches of voltage source inverters (VSIs) and thereby regulate the output voltage and frequency of TIMs [12]. The main advantages of the PWM techniques are that the power loss in switching devices is very low, high efficiency, low distortion, short computation time, and minimal harmonics [38]. PWM switching techniques include the SPWM, HBPWM, and RPWM. These switching techniques achieve satisfactory performance. However, in some cases, high computational time, harmonic distortion and switching loss create problems in TIM control. SVPWM switching technique is the best approach for minimizing switching loss and harmonic output signals from the inverter controller of TIM [5], [13]. The details of the PWM methods are explained in the next section.

A. SPWM SWITCHING TECHNIQUES

The SPWM technique is very popular in industrial converter applications because of its good performance and easy implementation. Its main principle is producing an AC voltage waveform at a desired frequency ($f_{control}$) (50 Hz or 60 Hz); subsequently, sinusoidal control signals are compared with a triangular waveform at a switching frequency (f_s) (Fig. 5). The control of the AC output voltage of the inverter is achieved by adjusting the control signal amplitude using the modulation index (MI). The MI is the ratio between the peak amplitude of the sinusoidal control signal ($V_{control}$) and the amplitude of the triangular waveform ($V_{triangle}$), as expressed

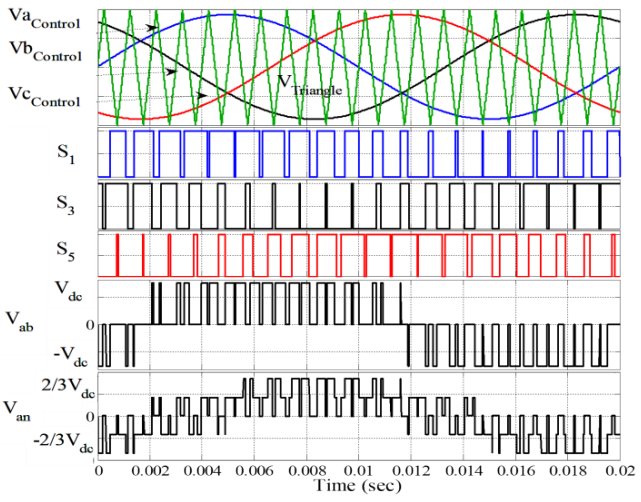

FIGURE 5. SPWM waves and voltages of a three-phase inverter.

in [39, eq. (21)]. The value MI can be varied from 0 to 1 to deliver a linear equation between the reference and the output wave.

$$MI = \frac{V_{control}}{V_{triangle}} \tag{21}$$

Fig. 5 shows the signals generation based on the comparison between the three-phase sinusoidal control waveform and the triangular waveform. This comparison is based on the condition $V_{control} > V_{triangle}$, in which case S = ON; otherwise, S = OFF. In a bipolar switching scheme, each switch works opposite to the facing switch, similar to the case involving the comparison of $V_{a\_control}$ with the triangle waveform to generate the PWM signal for $IGBT_1$ and the opposite $IGBT_4$ in leg1, which is the same as leg2 and leg3 [40].

The line-to-line voltage wave V_{ab} is given as $v_{ab} = v_{a0} - v_{b0}$. The corresponding line-to-neutral voltage wave (assuming a star-connected load) is given as $v_{an} = {}^2/_3 v_{a0} - {}^1/_3 v_{b0} - {}^1/_3 v_{c0}$ (Fig. 5). The disadvantage of this technique is the excessive switching loss caused by the high switching frequency and reduction of available voltage.

B. SVPWM SWITCHING TECHNIQUES

The SVPWM method generates PWM control signals in the three-phase inverter which is verified as the best technique for variable speed drive (VFD) applications. This approach has the improved technique to achieve a high output voltage, minimize the harmonic output, and reduce the switching losses relative to other PWM techniques. Therefore, the SVPWM technique is validated as the best method in terms of minimizing harmonic distortion [41], [42].

As shown in Fig. 5, the upper IGBTs (S_1, S_3, and S_5 are equivalent to 1) are switched on, whereas the corresponding lower IGBTs (S_2, S_4 and $S_6$are equivalent to 0) are switched off. The on and off states of the upper IGBTs (i.e., S_1, S_3 and S_5) can be used to determine the output voltage. The relationship between the positive switching variable and the line-to-line voltages (V_{ab}, V_{bc}, V_{ca}) as well as the line-to-neutral voltages (V_{an}, V_{bn}, V_{cn}) can be expressed as follows [43].

$$\begin{bmatrix} V_{ab} \\ V_{bc} \\ V_{ca} \end{bmatrix} = V_{dc} \begin{bmatrix} 1 & -1 & 0 \\ 0 & 1 & -1 \\ -1 & 0 & 1 \end{bmatrix} \begin{bmatrix} S_1 \\ S_3 \\ S_5 \end{bmatrix} \tag{22}$$

$$\begin{bmatrix} V_{an} \\ V_{bn} \\ V_{cn} \end{bmatrix} = \frac{V_{dc}}{3} \begin{bmatrix} 2 & -1 & -1 \\ -1 & 2 & -1 \\ -1 & -1 & 2 \end{bmatrix} \begin{bmatrix} S_1 \\ S_3 \\ S_5 \end{bmatrix} \tag{23}$$

The six IGBTs in the inverter can form eight switch variables. Six of these switch variables are non-zero vectors (i.e., $V_1, V_2 \ldots\ldots, V_6$), and the rest are zero vectors (i.e., V_0, V_7) selected for the three upper IGBTs switches. The on and off patterns of the lower IGBTs switches are opposite to those of the upper switches. The voltage space vectors ($V_0, V_1, \ldots\ldots, V_7$) are determined using (22) and (23). The eight switching vectors, output line-to-neutral voltages, and output line-to-line voltages are shown in Fig. 6 and Table 1 [44].

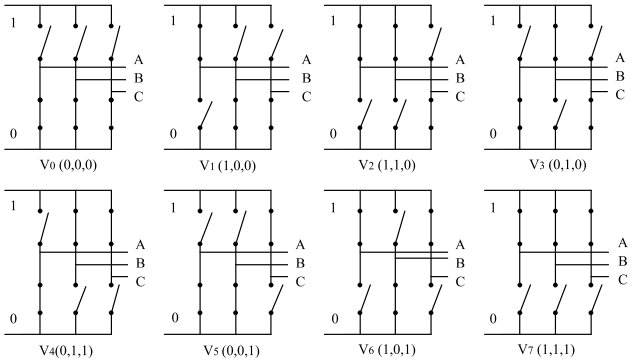

FIGURE 6. Eight states for the inverter voltage vectors (V_0 to V_7).

TABLE 1. Switching pattern of voltage space vectors with phase and line voltages.

Voltage vectors	Switching vectors			Line to neutral voltage			Line to line voltage		
	S_1	S_3	S_5	V_{an}	V_{bn}	V_{cn}	V_{ab}	V_{bc}	V_{ca}
V_0	0	0	0	0	0	0	0	0	0
V_1	1	0	0	$2/3\,V_{dc}$	$-1/3\,V_{dc}$	$-1/3\,V_{dc}$	V_{dc}	0	$-V_{dc}$
V_2	1	1	0	$1/3\,V_{dc}$	$1/3\,V_{dc}$	$-2/3\,V_{dc}$	0	V_{dc}	$-V_{dc}$
V_3	0	1	0	$-1/3\,V_{dc}$	$2/3\,V_{dc}$	$-1/3\,V_{dc}$	$-V_{dc}$	V_{dc}	0
V_4	0	1	1	$-2/3\,V_{dc}$	$1/3\,V_{dc}$	$1/3\,V_{dc}$	$-V_{dc}$	0	V_{dc}
V_5	0	0	1	$-1/3\,V_{dc}$	$-1/3\,V_{dc}$	$2/3\,V_{dc}$	0	$-V_{dc}$	V_{dc}
V_6	1	0	1	$1/3\,V_{dc}$	$-2/3\,V_{dc}$	$1/3\,V_{dc}$	V_{dc}	$-V_{dc}$	0
V_7	1	1	1	0	0	0	0	0	0

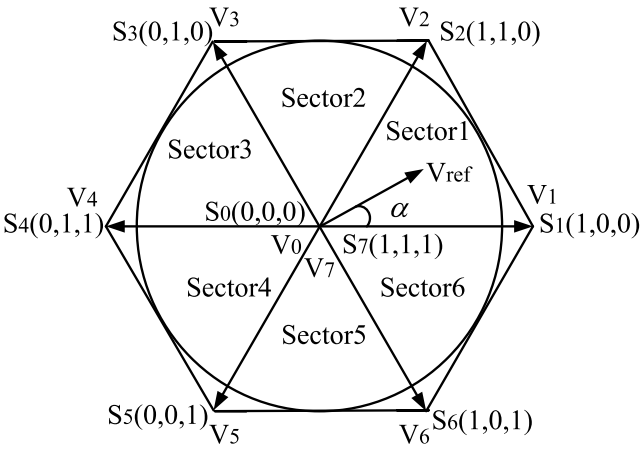

FIGURE 7. Space vector diagram.

The working principle of the SVPWM divides the output wave of the inverter into six sectors in a hexagon shape. Each sector lies between two voltage space vectors while the sector angle is 60 degrees apart (Fig. 7) [13], [15], [29].

The SVPWM technique receives a three-phase voltage (V_a, V_b, and V_c) separated by 120 degrees between two phases and converts it into two phases ($V\alpha$ and $V\beta$) with difference angle of 90 degrees using Clark's transformation (Fig. 8).

The two-phase voltages ($V\alpha$ and $V\beta$) are a mathematical transformation employed to simplify the analysis of three-phase voltage. The voltages are used to obtain the

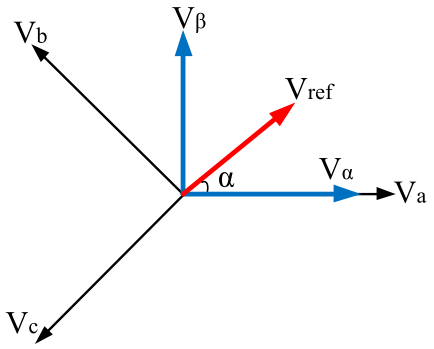

FIGURE 8. Space vector diagram.

magnitude of the reference voltage vector (V_{ref}) and the angle (α) between the voltage vectors in the hexagon. The V_{ref} is considered the magnitude of the Vα and Vβ voltages and the α is represent the frequency of the Vα and Vβ. V_{ref} and α are located between the two adjacent non-zero vectors and the zero vectors, and they can be calculated as follows [35].

$$\begin{bmatrix} V_\alpha \\ V_\beta \end{bmatrix} = \frac{2}{3}\begin{bmatrix} 1 & -\frac{1}{2} & -\frac{1}{2} \\ 0 & \frac{\sqrt{3}}{2} & -\frac{\sqrt{3}}{2} \end{bmatrix}\begin{bmatrix} V_a \\ V_b \\ V_c \end{bmatrix} \tag{24}$$

$$|V_{ref}| = \sqrt{V_\alpha^2 + V_\beta^2} \tag{25}$$

$$\alpha = \tan^{-1}\frac{V_\beta}{V_\alpha} \tag{26}$$

V_{ref} is in sector 1, and can be synthesised by the vectors adjacent to it in that sector.

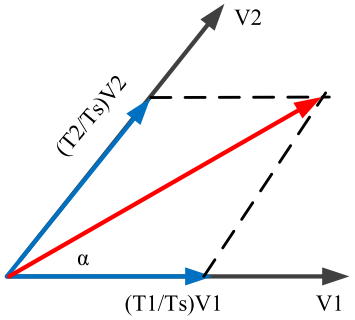

FIGURE 9. Space of sector-1 between V_1 and V_2.

Fig. 9 shows the corresponding space vectors and time durations (T_1, T_2, andT_0) in sector 1. The time duration of V_{ref} is calculated through the product of the reference voltage and its sampling time period equal to the sum of the voltages multiplied by their time interval of space vectors in the chosen sector as shown in the following [45].

$$\int_0^{T_s} \bar{V}_{ref}\,dt = \int_0^{T_1} \bar{V}_1 dt + \int_{T_1}^{T_1+T_2} \bar{V}_2 dt + \int_{T_1+T_2}^{T_s} \bar{V}_0 dt,\ T_s = T_1 + T_2 + T_0 \tag{27}$$

where T_s is the switching time calculated by $T_s = {}^1\!/_{f_s}$, and f_s is the switching frequency.

As shown in Eq. (27), $\bar{V}_0$ applies a zero voltage to the output load. Consequently, the equation becomes:

$$T_s\bar{V}_{ref} = T_1\bar{V}_1 + T_2\bar{V}_2 \tag{28}$$

Substituting the values of$\bar{V}_1$ and $\bar{V}_2$ from Table 1 to the $\alpha\beta$ frame and analyse the voltage vectors yield the following [40]:

$$T_s\left|V_{ref}\right|\begin{bmatrix}\cos(\alpha)\\ \sin(\alpha)\end{bmatrix} = T_1\frac{2}{3}V_{dc}\begin{bmatrix}1\\0\end{bmatrix} + T_2\frac{2}{3}V_{dc}\begin{bmatrix}cos\frac{\pi}{3}\\ sin\frac{\pi}{3}\end{bmatrix} \tag{29}$$

$$T_1 = T_s\frac{3}{2}\frac{|V_{ref}|}{V_{dc}}\frac{\sin\left(\frac{\pi}{3}-\alpha\right)}{sin\frac{\pi}{3}} \tag{30}$$

$$T_2 = T_s\frac{3}{2}\frac{|V_{ref}|}{V_{dc}}\frac{sin\alpha}{sin\frac{\pi}{3}} \tag{31}$$

The modulation index (MI) for the SVPWM is the relationship between the reference voltage magnitude and the DC voltage value shown in the following equation [14].

$$MI = \frac{|V_{ref}|}{\frac{2}{\pi}V_{dc}} \tag{32}$$

The time duration in the other sectors (n) can be calculated by substituting Eq. (32) into (30) and (31) and by using 60 degrees with α for each sector to become [46], [47]:

$$T_1 = \frac{\sqrt{3}.T_s.|V_{ref}|}{V_{dc}}\sin\left(\frac{n}{3}\pi - \alpha\right) \tag{33}$$

$$T_2 = \frac{\sqrt{3}.T_s.|V_{ref}|}{V_{dc}}\sin\left(\alpha - \frac{n-1}{3}\pi\right) \tag{34}$$

$$T_0 = T_s - (T_1 + T_2) \tag{35}$$

The four types of switching patterns are as follows: symmetric sequence, right aligned sequence, alternating zero vector sequence, and highest current not switched sequence [40]. All switching patterns must satisfy the following two conditions to minimize the device switching frequency. The change of the switching state from one to another involves only two switches in the same inverter leg. If either one of the switches is turned on, then the other must be turned off to reduce the switching frequency. The movement of V_{ref} from one sector to the next is achieved with the minimum number of switching to reduce the switching losses. Researchers have proven and recommended that the symmetric sequence method is the best method because it reduces the switching losses. Table 2 and Fig. 10 show the presses for the symmetric sequence for each sector [25].

Fig. 11 shows the SVPWM signal generation, inverter output voltages, and comparison of the three signals of the duty ratio waveform with the triangular waveform. This comparison is based on the condition$V_{DutyRatio} > V_{triangle}$, in which case S = ON; otherwise,S = OFF. In a bipolar switching scheme, each switch works opposite to the facing switch, similar to the case involving the comparison of the

TABLE 2. Switching time calculation at each sector.

Sector	Upper switching	Lower switching
1	$T_a = T_1 + T_2 + T_0/2$ $T_b = T_2 + T_0/2$ $T_c = T_0/2$	$\overline{T}_a = T_0/2$ $\overline{T}_b = T_1 + T_0/2$ $\overline{T}_c = T_1 + T_2 + T_0/2$
2	$T_a = T_1 + T_0/2$ $T_b = T_1 + T_2 + T_0/2$ $T_c = T_0/2$	$\overline{T}_a = T_2 + T_0/2$ $\overline{T}_b = T_0/2$ $\overline{T}_c = T_1 + T_2 + T_0/2$
3	$T_a = T_0/2$ $T_b = T_1 + T_2 + T_0/2$ $T_c = T_2 + T_0/2$	$\overline{T}_a = T_1 + T_2 + T_0/2$ $\overline{T}_b = T_0/2$ $\overline{T}_c = T_1 + T_0/2$
4	$T_a = T_0/2$ $T_b = T_1 + T_0/2$ $T_c = T_1 + T_2 + T_0/2$	$\overline{T}_a = T_1 + T_2 + T_0/2$ $\overline{T}_b = T_2 + T_0/2$ $\overline{T}_c = T_0/2$
5	$T_a = T_2 + T_0/2$ $T_b = T_0/2$ $T_c = T_1 + T_2 + T_0/2$	$\overline{T}_a = T_1 + T_0/2$ $\overline{T}_b = T_1 + T_2 + T_0/2$ $\overline{T}_c = T_0/2$
6	$T_a = T_1 + T_2 + T_0/2$ $T_b = T_0/2$ $T_c = T_1 + T_0/2$	$\overline{T}_a = T_0/2$ $\overline{T}_b = T_1 + T_2 + T_0/2$ $\overline{T}_c = T_2 + T_0/2$

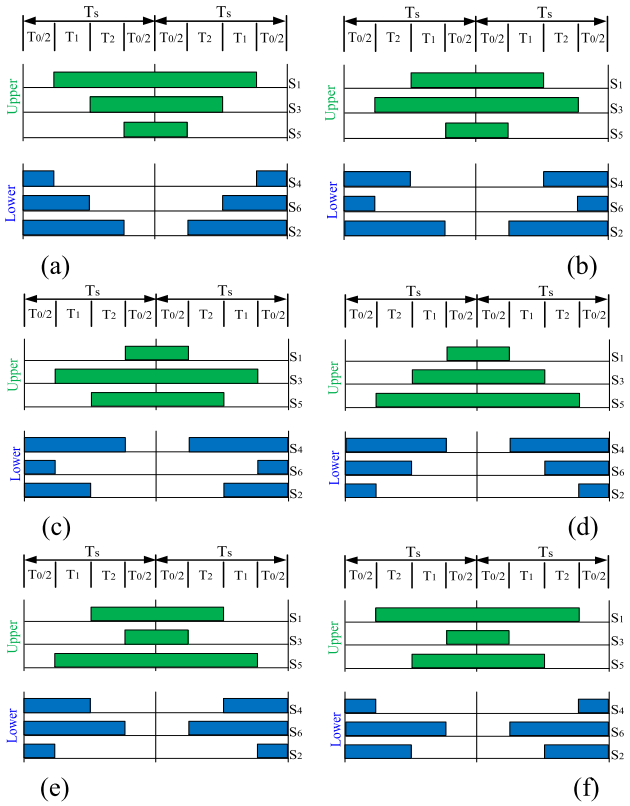

FIGURE 10. SVPWM switching patterns in (a) sector 1, (b) sector 2, (c) sector 3, (d) sector 4, (e) sector 5, and (f) sector 6.

$V_{Ta\_DutyRatio}$ with the triangle waveform to generate the PWM signal for $IGBT_1$ and the opposite $IGBT_4$ in leg1, which is the same as leg2 and leg3 [40].

Many researchers have applied the SVPWM technique in their systems to minimize the inverter harmonic waveform and improve performance [5]. Researchers have also used the SVPWM with the V/f control strategy based on the ANN controller in the TIM [48], [49]. The SVPWM is applied in Indirect field oriented control (IFOC) of a TIM and is executed with an FLC to control the PV grid inverter system [39]. The SVPWM technique with the sliding mode control method is implemented for the torque control of the TIM [50], [51]. The SVPWM with sensorless control is used to control for high-speed surface permanent magnet synchronous motor (PMSM) drives based on V/f control [49]. V/f control is used the SVPWM technique for three-level VSI in the V/f control for high-power variable speed drive [52]. The SVPWM is also employed with the FLC to adjust the position loop for the vector control of the IM drive [53]. The Direct torque control (DTC) is used with the SVPWM technique to improve and minimize the torque ripple for an induction machine [54]. The PMSM drives use the SVPWM to control torque and flux in the vector control [55]. The ANN with the SVPWM based on sensorless control estimates the rotor speed in the vector control of the TIM drive [56]. However, the SVPWM requires a complex online computation, which leads to difficulty in real-time implementation. Therefore, the conventional SVPWM requires additional memory that limits the selection of switching frequency, thereby reducing its accuracy [57], [58]. Some researchers have solved this problem and have improved the power quality problem by utilizing the GA-based SVPWM [53], ANN-based SVPWM for two-level inverter [55], ANN-based SVPWM for three-level inverter [14], [16], and the ANFIS-based SVPWM used for two-level inverters [15].

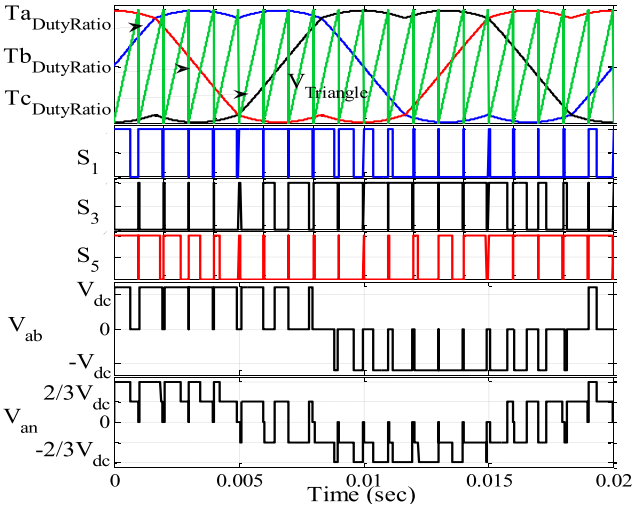

FIGURE 11. SVPWM waves and voltages of a three-phase inverter.

IV. IM INTELLIGENT CONTROLLER TECHNIQUES

A. SCALER CONTROL

The scalar control was introduced in 1960 for TIM control [59]. The V/f control is based on the open and closed

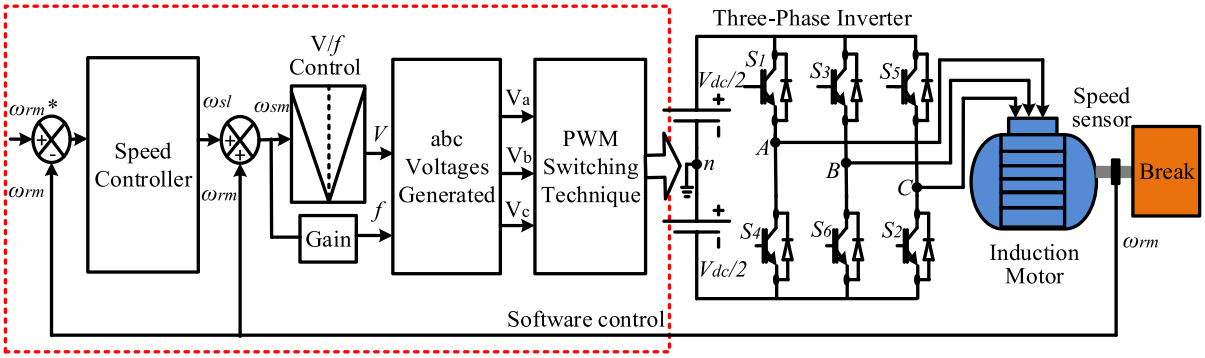

FIGURE 12. Closed loop of scalar control for TIM drive.

loop control system of the IM speed [60] while the variable voltage and frequency of the TIM is a closed loop control system [61]. The V/f control method is applied to TIM drives to achieve the dynamic response and stable performance of the IM. This strategy delivers many benefits including simple design and structure, cheap price and have a minor steady-state error. Moreover, the starting current requirement is low. The acceleration and deceleration can also be controlled by controlling the change of the supply frequency. The main advantage of V/f control is that it does not need parameters for IM implementation. It is utilized to regulate the supply voltage magnitude of the IM, and it is demonstrated as the best selections for variable torque and speed applications [27]. The V/f control keeps the ratio of scalar voltage and frequency unchanged which maintains the maximum magnetic flux in the air gap. Voltage and frequency do not hold any explicit relationship, however, the relationship between voltage and frequency can be developed by the flow of electromagnetic flux which can be expressed follows [3].

$$\psi_m \cong \frac{V_p}{f} \cong K_v \tag{36}$$

where ψ_m is the maximum air gap flux, V_p is the maximum phase voltage, and K_v is the ratio of V_p to f.

The block diagram of the V/f control method and the slip speed (ω_{sl}) is presented in Fig. 12 which shows the calculation of the change in speed using TIM characteristics. This slip speed control is added with ω_{rm} to generate ω_{sm}. The synchronous speed is then converted to a synchronous frequency to generate the peak voltage using V/f control. The main limitation of this control is its low performance in low speed operations [3], [7], [62].

B. VECTOR CONTROL

Vector control is the most commonly used method in many applications because of its high performance for controlling IMs. The principle of the vector control is based on obtaining the magnitude and phase of voltages or currents to control IMs. Thus, vector control is based on controlling the position of the flux, voltage, and current vectors of the IM. This control is carried out depending on the Clark and Park transformations, which are responsible for generating torque and flux, respectively. An IM does the similar operation like a separately excited DC motor drive in which the armature and field currents control the torque and flux respectively [63]–[65]. This characteristic results in disadvantageous coupling between electromagnetic torque and flux, which leads to difficult use and complexity of IM controllers [7], [66].

This problem can be solved by using Field oriented control (FOC) as shown in Fig. 13. Table 3 shows a comparison between the performance of scalar and vector control in IM.

TABLE 3. Comparison between scalar and vector control.

	Scalar control	Vector control
1.	Simple structure	Complex structure
2.	Low cost and easy design in prototype implementation	High cost and difficult design in prototype implementation
3.	Normal performance and low performance a low-speed conditions	High performance in FOC and low performance of DTC in a low-speed response
4.	Dose not requires identification of IM parameters	Requires and sensitive to IM parameters
5.	Requires one sensor, that is, speed sensor.	Require many sensors, such as six sensors in DFOC, four sensors in IFOC, and six sensors in DTC
6.	Minimizes current ripple.	High current ripple in DTC
7.	Does not require coordinate transformations	Requires a coordinate transformation in FOC

TIMs are in general complex, nonlinear, and multi-variable systems. Scalar and vector control methods can overcome TIM control problems, but these methods do not meet the required accuracy to control TIMs. Therefore, Scalar and vector control approaches need advanced controller techniques for the proper adjustment of current, voltage, flux, speed and torque of the IM [29], [40], [67]. These controller techniques can be divided into two groups such as conventional controllers and AI controllers [68]–[70].

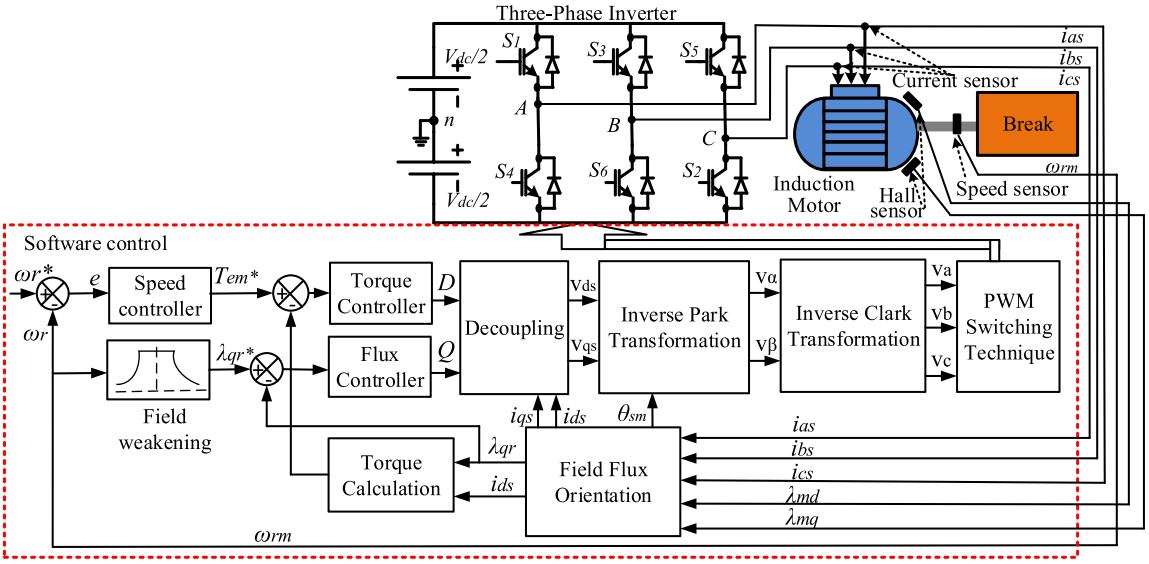

FIGURE 13. Block diagram of FOC for TIM drive.

C. CONVENTIONAL CONTROLLER

There are different categories of conventional controllers such as PI, PD and PID controllers to regulate Speed, torque, current and voltage. Of these, the PID controller is considered as most efficient control method recommended by Taylor Instrument Company in 1936 [71]. PID controller has a simple structure, easy design, low cost and is extensively used to control MI in the industrial application [72]–[74]. The structure of a PID controller is shown in Fig. 14 that takes measured signal and reference value to obtain the error signal for controlling signals such as an error in speed, torque, flux, current, or voltage.

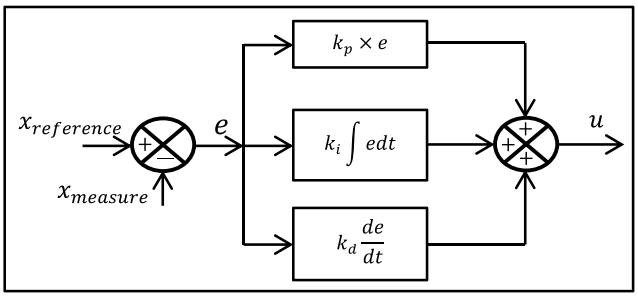

FIGURE 14. Structure of PID control.

The output signal of this controller contains the sum of errors that include proportional, integral and derivative of that error, as presented in the equation below:

$$u(t) = K_p e(t) + K_i \int_0^t e(t)\,dt + K_d \frac{de(t)}{dt} \qquad (37)$$

where e is the error $e = (x_{refrence} - x_{measure})$, u presents the output signal, K_p, K_i, K_d are the proportional, integral and derivative gain respectively. The performance of the PID can be enhanced using selective PID parameters. Each parameter plays an important role in controlling the IM as shown in the Table 4.

TABLE 4. Characteristics of PID control parameters.

Type	Rise time	Overshoot	Settling time	Steady state error
K_p	Decrease	Increase	Small change	Decrease
K_i	Decrease	Increase	Increase	Eliminate
K_d	Minor change	Decrease	Decrease	No effect

Though PID controller has a simple structure, it has many shortcomings, such the model is very sensitive to temperature and model parameters variation. Also, the model needs mathematical computation and has a rapid change in reference speed and load disturbances. Furthermore, The selection of the suitable parameters to improve the stability is a laborious task [21], [75]–[77]. Therefore, many approaches have been introduced to find PID parameters including Cohen-Coon method, Lambda tuning method, Ziegler-Nichols method [78], [79], and visual loop tuning method, and so on. However, these approaches have some drawbacks such as need a mathematical model and some calculation operations, some trial-and-error and process upset. Therefore, several optimization techniques have been proposed to find the optimal parameters of PID controller [80].

The TIM control systems have been researched in many studies. The V/f control strategy with PID controller is applied in stand-alone squirrel cage induction machine for wind power application [81]. The PMSM drives use PID controller to regulate the power factor angle [60]. In [82] and [83] the PID controls DFIG (doubly fed induction generator) of a wind power plant. PI control is introduced in IFOC in a single-phase IM. The vector control uses PI controller

to calculate the stator resistance of a single-phase IM [84]. PI controller with FOC is suggested to detect the faults in the sensor of an IM [85]. The PI control is proposed to decline the cost of solar cells in PV applications [86]. PI control uses IFOC for a five-phase IM to analyze the third harmonic injection [87]. PID controls the flux and torque to reduce the torque ripple in DTC for IM drive [88]–[90]. PI control is also applied to interconnected thermal power system [72].

D. ANN CONTROLLER

The AI based controllers have been applied in numerous applications. ANN is an information processing system that has certain performance properties in common with biological neural networks. ANN has improved mathematical models of human cognition or neural biology [91]. The structure of ANN can be divided into three layers. Each layer comprises of many neurons or nodes with activation functions, such as linear, unsigmoid and sigmoid functions. The ANN structure consists of three layers which are known as the input layer, the hidden layer, and the output layer. The input layer has nodes number, which is dependent on the number of inputs $(x_1, x_2, \ldots, x_n)$, hidden layers of N-nodes and the output layer of outputs $(t_1, t_2, \ldots, t_m)$ as shown in Fig. 15. There are weights and bias between input layer and hidden layer as well as hidden layer and output layer [92].

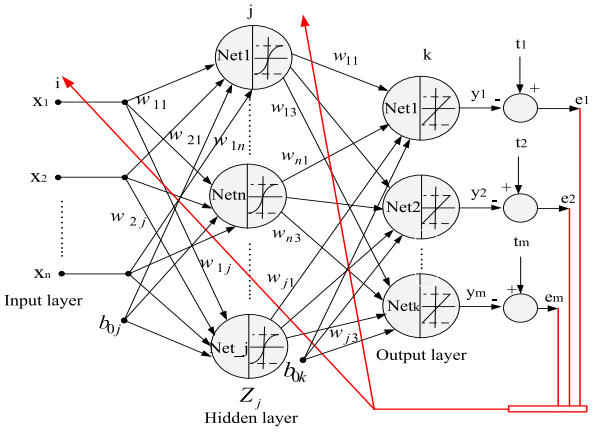

FIGURE 15. Design of ANN-BP structure.

The node (neuron) consists of two parts which are net function and activation function as shown in Fig. 16. There are three types of activation function namely, linear, unsigmoid (binary sigmoid) and sigmoid (bipolar sigmoid) function.

The back-propagation (BP) network training algorithm involves three stages namely, the feed-forward of the data training pattern, BP of the associated error, and the adjustment of the weights. The ANN is trained through the batch mode and the training data is used for training ANN which is taken from the system. The training data consider of input $(x_1, x_2, \ldots, x_n)$ and target output $(t_1, t_2, \ldots, t_m)$. Fig. 15 shows the ANN structure, training procedure and the adjustment of the weights. The feed-forward stage begins with receiving each input signals (x_i) and sending it to the

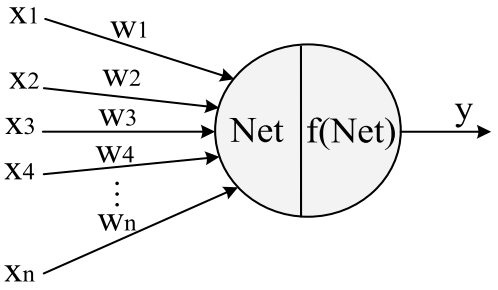

FIGURE 16. Structure of node (neuron).

each of the hidden nodes $(Z_1, \ldots, Z_j)$. Each hidden node computes net function and activation function by using [93]

$$net_j = b_{0j} + \sum_{j=1}^{P} w_{ij} X_i \tag{38}$$

$$Z_j = f\left(net_j\right) \tag{39}$$

where, x_i, $i = 1, 2, \ldots, n$ is the inputs, Z_j, $j = 1, 2, \ldots, P$ is the outputs hidden layer, w_{ij} is the weights between the input layer and hidden layer and b_{0j} is the bias between the input layer and hidden layer. Each nodes in the hidden layer have activation functions [94]. Then, the outputs of hidden nodes (Z_j) are sent to each output nodes. Each output node (y_k) computes net function and activation function by using [92]:

$$net_k = b_{0k} + \sum_{k=1}^{n} w_{jk} Z_j \tag{40}$$

$$y_k = f\left(net_k\right) \tag{41}$$

where, $y_k, k = 1, 2, \ldots, h$ is the outputs of the final layer, w_{jk} is the weight between the hidden layer and output layer and b_{0k} is the bias between the hidden layer and output layer.

The procedure of BP training algorithm begins with the generation of small value weights for all network. The error is computed for each output unit of ANN by subtracting output ANN (y_k) from the target data (t_k) using the formula $(e_k = t_k - y_k)$. The error is based on the calculation of the factor (δ_k). δ_k distributes the error at the output unit (y_k) and operates to the update all data for previous layers as shown in following equation [94].

$$\delta_k = error_k f'\left(net_k\right) \tag{42}$$

Change of weights (Δw_{jk}) between hidden layer and output layer is computed by δ_k and the change of bias weights (Δb_{0k}) is calculated as [93],

$$\Delta w_{jk} = l_r \delta_k Z_j \tag{43}$$

$$\Delta b_{0k} = l_r \delta_k \tag{44}$$

where l_r is the learning rate. The factor δ_j is calculated in the hidden layer. It is dependent on δ_k and derivative of its activation function as shown in the following equation,

$$\delta_j = f'\left(net_j\right) \sum_{k=1}^{n} w_{jk} \delta_k \tag{45}$$

Change of weights (Δw_{ij}) between input layer and hidden layer is computed by δ_j and the change of bias weights (Δb_{0j}) is caculated by the following equations [93]

$$\Delta w_{ij} = l_r \delta_j X_i \tag{46}$$
$$\Delta b_{0j} = l_r \delta_j \tag{47}$$

The final step is updating the weights and bias weights by using the following equations [93],

$$w_{ij}\,(new) = w_{ij}\,(old) + \Delta w_{ij} \tag{48}$$
$$b_{0j}\,(new) = b_{0j}\,(old) + \Delta b_{0j} \tag{49}$$
$$w_{jk}\,(new) = w_{jk}\,(old) + \Delta w_{jk} \tag{50}$$
$$b_{0k}\,(new) = b_{0k}\,(old) + \Delta b_{0k} \tag{51}$$

ANN has recently been used as an intelligent controller to control IMs to estimate IM parameters, and to detect faults in IMs because it does not require mathematical models and it achieves good prediction for control compare to conventional controller. However, ANN controllers require massive data and longtime training and learning [95]. ANN controllers have been used in previous research, such as in [4], to estimate the speed of scalar IM control. Four ANN-based switches are adopted in a three-phase VSI using SVPWM [5]. The ANN-based implementation of the SVPWM of a three-phase neutral-point clamped bi-directional converter is realized to improve power quality [15]. ANN controller is used to estimate the torque of IM drives [96]. In [15], the ANN-based SVPWM is applied to minimize the complex computation of a three-level inverter. The ANN controller in a wind generator is based on a speed controller [97]. ANN is also used as a speed controller in IFOC for IM drive [98], [99] and DTC IM drive [47]. ANN is based on monitoring negative sequence voltages and three-phase shift [100]. In [101], an ANN controller is used to control a linear IM. This controller is also used in the base fault identification scheme implementation for IMs [102].

E. ANFIS CONTROLLER

Fuzzy system and neural network have their own merits and demerits. This fact leads to the increased interest in combining fuzzy and neural networks to take advantage of their various properties; such combination generates a new method called the ANFIS. The ANFIS structure consists of many layers [14], [103]. The ANFIS has recently been used as an intelligent controller with scalar and vector control for controlling and estimating IM parameters without a mathematical model, and achieves a good performance for controlling any sudden change in speed or load. However, ANFIS has shortcomings such as it requires huge data, has the complex computational burden and needs a long time for data training and learning [104], [105].

The first order Takagi-Sugeno fuzzy model used is a typical rule set with number of inputs $(x_1, x_2, \ldots, x_n)$ and a function response of $f_1, f_2, \ldots\ldots, f_n$ which can be given in generalized form as [106].

Rule 1: If x_1 is A_1 and x_2 is B_1 then $f_1 = p_1x_1 + q_1x_2 + r_1$

$\vdots$

Rule n: If x_n is A_i and x_n is B_i then $f_i = p_ix_n + q_ix_n + r_i$ where A_i, B_i are the parameters of the non-liner membership functions (MFs) for inputs $(x_1, x_2, \ldots, x_n)$ and p_i, q_i, r_i are parameters of the linear activation function. The ANFIS architecture consists of five layers, namely, the fuzzy layer (layer1), product layer (layer2), normalized layer (layer3), defuzzification layer (layer4), total output layer with rules (layer5) and MFs connected with each input. For example, Fig. 17 shows the ANFIS structure for two inputs [14], [22], [107].

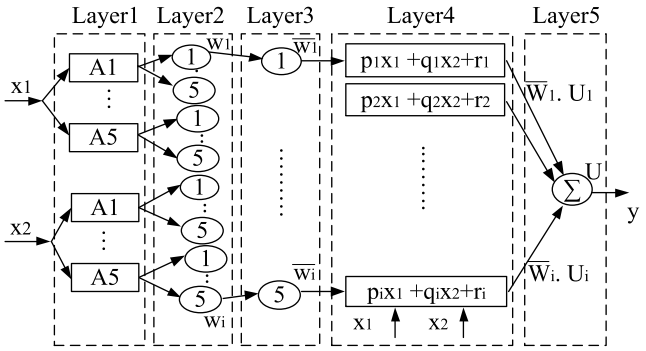

FIGURE 17. ANFIS architecture.

Layer 1: In this layer, the input values x_1 and x_2 are an intervention for each node from A_i and B_i. A_i and B_i are the linguistic variables used in fuzzy theory to define MFs. The triangular and gbell functions are expressed as in following equation [22].

$$\mathrm{F}(x; a, b, c) = \begin{cases} \dfrac{x-a}{b-a} & a \le x < b \\ \dfrac{x-c}{b-c} & b \le x < c \end{cases} \tag{52}$$

$$F\,(x; a, b, c) = \frac{1}{1 + \left|\frac{x-c}{a}\right|^{2b}} \tag{53}$$

where a, b, and c are the parameters that set limits for triangular and gbell MFs. The output of each node in this layer is O'_{1i}, and is given by,

$$O'_{1i} = \mu A_i\,(x_1) \quad and \quad O'_{1i} = \mu B_i\,(x_2) \tag{54}$$

Layer 2: This layer consists of 25 nodes. Each node is a product of the multiplied between the MFs for first input x_1 and MFs for second input x_2 as follows,

$$O'_{2i} = w_i = \mu A_i\,(x_1) \quad AND \quad \mu B_i\,(x_2) \tag{55}$$

Layer 3: The output of this layer is the normalized firing strength in each node as shown in the following equation,

$$O'_{3i} = \bar{w}_i = \frac{O'_{2i}}{\sum\limits_i O'_{2i}} \tag{56}$$

Layer 4: This layer calculates the output using input contribution of each nth rule which is expressed as,

$$O'_{4i} = \bar{w}_i U_i = O'_{3i} \sum_{i=1}^{p} p_i x_1 + q_i x_2 + r_i, \quad i = 1, 2, \ldots\ldots, p \tag{57}$$

Layer 5: This layer consists of one node to calculate the sum of the output from layer 4 as shown below.

$$O'_{5i} = \sum O'_{4i} \tag{58}$$

The main objective of the ANFIS learning algorithm is to tune the premise parameter (a_n, b_n, c_n) and the consequent parameters (p_n, q_n, r_n), so that the ANFIS output is compatible with the training data. Least square estimation (LSE) algorithm is adopted to determine the optimal solutions of the consequent parameters. When the premise parameters are changeable, a hybrid algorithm which is a combination of gradient descent back-propagation and LSE algorithms is used to solve the problem. The hybrid algorithm consists of two passes which are forward pass LSE and backward pass (gradient descent). The forward pass is implemented mainly to find the optimize values the consequent parameters when the premise parameters are constant while the function of the backward pass is used to optimize the premise parameters. It has been demonstrated that the hybrid algorithm is very effective in training the ANFIS [108].

ANFIS was used to control a PV inverter for minimizing the total harmonic distortion (THD) in the output signals and the speed of the DC motor [23]. In [14], an ANFIS-based SVPWM is employed for IM drive. An ANFIS controller is used to improve the speed controller for IM in V/f control [17]. The ANFIS is also used to improve the compensation capability of a unified power quality conditioner [107]. The DTC of an IM drive is controlled and enhanced with the ANFIS [109]. ANFIS is also used to control a stepping motor drive [110]. An ANFIS controller is applied for speed control in an IM [111]. This controller is used to detect inter turn insulation in stator and faults in bearing wear in a single-phase IM. ANFIS is applied with IFOC to improve the performance of IM drive [112].

F. FUZZY LOGIC CONTROLLER

The design principle of Fuzzy logic controller (FLC) comprises of four steps, namely, fuzzification, rule base, inference engine, and defuzzification. Fuzzification analyzes the every input into a group with convenient linguistic values as shown in [114, Fig. 18].

1) DEFINATION OF THE MODULE CHARACTERISITCS

The first step signifies the number of inputs, outputs and position of fuzzy MFs based on knowledge. The input data includes an error (e) and change of error (de) as shown in the following equations.

$$e(t) = x_n^* - x_n \tag{59}$$

$$de(t) = e(t) - e(t-1) \tag{60}$$

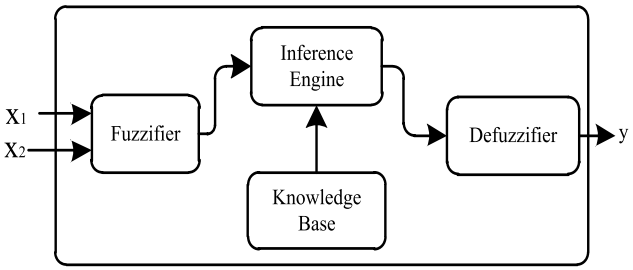

FIGURE 18. Structure of the fuzzy logic controller.

2) FUZZIFICATION DESIGN

The second step characterizes the inputs with appropriate linguistic value by evaluating every input into a group. This step is known as a unique MF label, symbolizing "big", "medium" or "small". Hence, the accuracy of FLC is highly reliant on a number of MFs used in the linguistic label. The errors and change in error in MFs are represented as trapezoidal and triangular MFs. In Fig. 19(a), MFs for error $\mu_e(e)$ contains three variables (A_0, A_1, A_2) while in Fig. 19(b), MFs for change of error $\mu_{de}(de)$ comprises three variables (B_0, B_1, B_2). The mathematical equation of MFs can be expressed using Eq. (61) and (62),

$$\mu_e(e) = \begin{cases} \dfrac{e - A_0}{A_1 - A_0} & A_0 \le e < A_1 \\ \dfrac{e - A_2}{A_1 - A_2} & A_1 \le e < A_2 \end{cases} \tag{61}$$

$$\mu_{de}(de) = \begin{cases} \dfrac{de - B_0}{B_1 - B_0} & B_0 \le de < B_1 \\ \dfrac{de - B_2}{B_1 - B_2} & B_1 \le de < B_2 \end{cases} \tag{62}$$

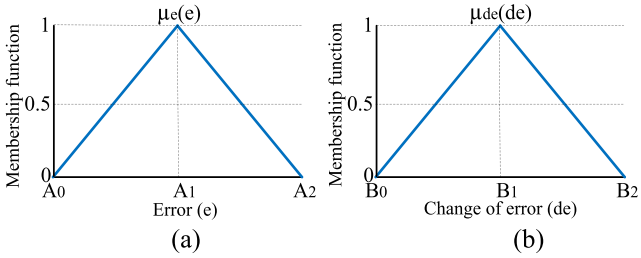

FIGURE 19. Triangular of membership functions.

There would be a significant improvement in the performance of FLC if the appropriate MFs is chosen. The conventional FLC uses trial and error method to determine the MFs which is difficult to obtain because of its complex mathematical calculation and it needs time and effort to find the boundaries.

3) INTERFACE ENGINE DESIGN

The third stage indicates decision making using control rules and linguistic terms. Generally, inference systems are categorized into two classes namely, Mamdani and Takagi-Sugeno. Mamdani method is used in common due to its

simple design and easy structure. The if-then linguistic term is used as a fuzzy rule. The fuzzy rule operates the output MFs related between the inputs (e, de) and the output (ω_{sl}) [38], [142]. The rules are expressed in the following equations and details of the 49 rules are shown in Table 5.

Rule 1: If e is "Ne3" and de is "Nde3" THEN u is "NB".
Rule 2: If e is "Ne3" and de is "Nde2" THEN u is "NB".

⋮

Rule 48: If e is "Pe2" and de is "Pde3" THEN u is "PB".
Rule 49: If e is "Pe3" and de is "Pde3" THEN u is "PB".

TABLE 5. Fuzzy rules base.

de \ e	Ne3	Ne2	Ne1	Ze	Pe1	Pe2	Pe3
Nde3	NB	NB	NB	NB	NM	NS	Z
Nde2	NB	NB	NB	NM	NS	Z	PS
Nde1	NB	NB	NM	NS	Z	PS	PM
Zde	NB	NM	NS	Z	PS	PM	PB
Pde1	NM	NS	Z	PS	PM	PB	PB
Pde2	NS	Z	PS	PM	PB	PB	PB
Pde3	Z	PS	PM	PB	PB	PB	PB

NB: Negative big; NM: Negative medium; NS: Negative small; Z: Zero; PS: Positive small; PM: Positive medium; PB: Positive big.

4) DEFUZZIFICATION DESIGN

The final step in the FLC is known as Defuzzification. This controller generates the output values in this stage as a crisp value. Moreover, this process performs some adjustment and controls the crisp value of the output MFs. Nevertheless, these MFs are required to choose the number of the MFs and boundaries. The optimal value of MFs is found through trial-and-error method [22], [114].

$$O_{crisp} = \frac{\sum_i^n w_i \cdot u_i}{\sum_i^n w_i} \tag{63}$$

where n presents the number of rules, u presents the value of output MFs and w is the weights coefficient. The weights are estimated based on minimum value between $\mu_e(e)$ and $\mu_{de}(de)$ as presented in the equation below:

$$w_i = \min\left[\mu_e(e), \mu_{de}(de)\right] \tag{64}$$

A number of researchers have proposed to use FLC due to its ease of implementation, does not depend on a mathematical relationship, and can handle linear and non-linear systems based on linguistic rules, in which a large number of system variables can be evaluated. The FLC outperforms others controllers in terms of the improved control system and rapid transient control and reduction. However, the performance of FLCs is subject to appropriate selection of the MFs, the number of rules, and the rule base. A trial and error technique can be applied to calculate the variables which consumes a lot of time [75], [77].

FLC is used for speed controller of induction machine to improve V/f control [62], [12]. A FLC is used in an IM for different applications in vector control [115], and in DTC [24], [116]. The V/f control using FLC of an IM is used for achieving power level in a DC grid power system [117]. A FLC with the IFOC of a double star induction machine is used to enhance system performance under different operating conditions [87]. In [118], a new speed control for IM is developed by combining a FLC and phase plane theory [119]. A speed controller in IFOC for IM is designed using FLC and speed estimation [120], [53]. Another FLC is used to solve the torque and speed tracking problems of a doubly-fed IM [121]. In [122], a FLC is applied with IFOC to control the SVPWM of a three-level inverter of IM. FLC with a multi-scale entropy algorithm is used to predict the stator winding fault in IM [123]. FLC is also used in wind turbine to control a variable speed based on a dual star induction generator [124], [125]. In [126], speed control system for wind power generation system has been developed and improved using a FLC. In [127], a FLC-based steady state analysis is conducted for a wind driven single-phase single-winding self-excited induction generator. A FLC-based IFOC is performed to control five-phase IM drives [128]. A FLC-based speed controller in DTC for IM drives is utilized to improve dynamic responses [129], and IFOC for IM [130]. Another FLC-based speed controller is adopted to enhance the performance of a PMSM [131], [132]. In [133], a FLC-based current controller is used to improve the performance of a DC motor. A FLC is applied to a three-level inverter of IM [134]. In [135], a FLC is used to determine the inverter turn-off angle for optimum torque output. In [136], comparisons have been conducted between the use of a conventional PI and FLC for an IFOC of an IM drive. In [137], an online self-tuning FLC is proposed for the IFOC of an IM drive.

Moreover, FLC is also used to solve the PID control problem by searching for the best parameter values, [77], [21], [138] to tune up PID parameters in IFOC for IM. By using the speed error and its derivative, it is possible to eliminate the overshoot, achieve minimal rise time, and reduce the effect of load disturbance. A FLC based PI controller is also employed in IFOC for controlling the position of IM drive [53], for minimizing errors in networked control [139], and for regulating the load frequency in multi-area power systems [140].

Table 6 shows a comparative performance among conventional, ANN, ANFIS, and FLC controllers for a TIM drive.

V. INTEGRATED CIRCUITS FOR INDUCTION MOTOR CONTROL

The experimental control systems for IM drive can be implemented using microcontrollers, dSPACEs, FPGAs and DSPs. Different microcontrollers are used in many applications, which include microcontroller based on a fuzzy speed controller [141], fuzzy logic sensorless maximum power point tracking (MPPT) controller for wind energy conversion systems [142]. However, these microcontrollers have disadvantages such as a low memory that prevent them from writing large programs as well as low processing speed.

TABLE 6. Comparison of controller techniques.

No.	Conventional Controller	ANN Controller	ANFIS Controller	FLC Controller
1.	Simple structure and easy design	Normal structure and moderately complex design	Complex structure and moderately complex design	Simple structure and easy design
2.	Requires a mathematical model	Does not require a mathematical model	Does not require a mathematical model	Does not require a mathematical model
3.	Does not need a learning step	Needs a learning step and big data to train	Needs a learning step and big data to train	Does not need a learning step
4.	Good performance if the best values of PID parameters are found	Good performance if suitable data training, nodes number and activation functions are selected	Good performance if suitable data training and number and type of MFs are selected	Strong performance if the best boundaries for input and output MFs are selected

A number of dSPACE controller platforms have been used in many applications; for example, fuzzy vector control scheme is used for controlling IM, and grid interactive VSI [143]. dSPACE is also used for the ANFIS based SVPWM technique for VSI, and neutral-point clamped high-power factor converter [22]. In [144], dSPACE-based dynamic sensorless control is implemented for high-speed surface PMSM drives. SVPWM is used to minimize the harmonics in three-phase multi-level voltage source converters, and a digital control scheme based on dithered sigma delta modulation is implemented in the dSPACE board [145]. dSPACE is applied to develop the V/f control system for PMSM drives, IM drive, and parameters identification [60], [146]. In [147], IFOC is implemented for single-phase IM drive using a dSPACE control board. dSPACE is used to implement a sensorless IFOC for a single-phase IM drive with stator resistance tuning. A dSPACE-based fuzzy IP-self-tuning controller is adopted for IM speed control [138]. A dSPACE-based DTC is used for a three-level inverter-fed IM drive [148]. A real-time discrete nonlinear neural identifier employing recurrent high-order neural network is implemented in dSPACE [101]. An ANN-based adaptive estimator of rotor speed in a sensorless vector-controlled IM drive is applied by using a dSPACE board [56]. In [136], a FLC is implemented in IFOC for IM drives using a dSPACE control board. The fuzzy logic hysteresis-based DTC scheme of an IM is implemented in a dSPACE board [116]. The ANFIS controller based speed control of an IM drive is applied by using dSPACE [149].

A FPGA is implemented in many controller platforms; for example, FPGA based fuzzy sliding-mode controller is implemented for a PMSM drive [132]. The FPGA based on-line ANN is used as a speed controller for the selective harmonic elimination in PWM technique for IM [150]. ANNs have been implemented in FPGA for detecting multiple combined faults using the start-up vibration signals of a rotating machine [151]. In [152], the FOC of an IM drive is designed and implemented using a FPGA device. A FPGA-based multi-channel vibration analyzer is used for industrial applications in IM failure detection [153]. FPGA is also implemented in stepper motors for digital control [154]. However, the disadvantages of dSPACE and FPGA include their high cost inability to function under the standalone mode in a given system and need to be connected to a computer all the times.

DSP controllers are used in many applications because of their fast computation in comparison with other controllers, low power consumption, short design cycle, embedded processor, high density, affordability, and capability to function without a computer [74], [155]. As a result, DSP dominates in numerous applications. For example, a DSP is used to control a stable super-high-speed PMSM [156]. The SVPWM algorithm for three-level cascaded H-bridge inverter is implemented by DSP [157]. A DSP-based DTC is used for the torque ripple minimization of a VSI fed induction machine [158]. A DSP is implemented for controlling viable flux and torque as well as minimizing torque ripple for IM drive [159]. A DSP-based genetic PI speed controller is implemented for the speed loop of a brushless direct current (BLDC) motor [160]. DSP-based torque control is also implemented to DC motor [161]. A DSP-based DTC is used for a three-level inverter-fed IM drive [162]. A sensorless PMSM drives with DSP control is employed for operating speed in a wide range [155]. A DSP-based FLC is used to control the speed of an IM drive [120], to manage the position loop for vector control for IM [163], to improve the speed control of IM [164], and enhance the PID speed controller for PMSM [74]. A DSP-based ANN controller is utilized to estimate the speed of an IM driven by a VSI [4], to balance the capacitor voltage of a three-phase three-level power quality converter with SVPWM [165] [166], to model torque estimation for an open-loop induction machine [167], and to estimate the sensorless speed in indirect vector control for IM [168]. A DSP-based ANFIS controller is adopted to control IM speed [169] and DC motor [23], and to improve the V/f control of IM [170]. Table 7 presents a comparison

TABLE 7. Comparison among integrated circuits.

No.	Microcontroller	dSPACE	FPGA	DSP
1.	Low cost	High cost	High cost	Low cost
2.	Low memory	High memory	High memory	High memory
3.	Medium processor	Fast processor	Fast processor	Fast processor
4.	Standalone operation	Must be connected to a PC	Must be connected to a PC	Standalone operation
5.	Some versions can build the software from MATLAB	All versions can build the software from MATLAB	All versions can build the software from MATLAB	All versions can build the software from MATLAB

TABLE 8. Comparison of TIM drive under different control systems, controller techniques, PWM switching techniques, platforms and settling time.

Reference	PWM switching	Control system	Controller technique	Platform	Settling time (s)
[136]	HBPWM	IFOC	FLC	Matlab/Simulink	0.55
				dSPACE	6
[172]	HBPWM	IFOC	PI	Matlab/Simulink	0.8
				DSP	8
[21]	SPWM	IFOC	FLC-PI	DSP	1.2
[21]	SPWM	IFOC	PI	Matlab/Simulink	2.5
				DSP	3
			FLC-PI	Matlab/Simulink	2.2
				DSP	3.5
[173]	SPWM	IFOC	PI	Matlab/Simulink	0.55
			FLC-PI		0.5
[174]	SPWM	IFOC	ANFIS	Matlab/Simulink	0.95
				dSPACE	1.45
[175]	HBPWM	IFOC	ANFIS	Matlab/Simulink	1
				DSP	7
[176]	HBPWM Multilevel inverter	IFOC	Type-2 FLC	Matlab/Simulink	0.3
[177]	HBPWM	DTC	FLC-PI	Matlab/Simulink	0.112
			FLC		0.1
			Fuzzy sliding		0.095
	SVPWM	IFOC	PI	Matlab/Simulink	1
[181]	SPWM	IFOC	PI	DSP	1.5
[182]	SVPWM	IFOC	PI	DSP	0.85
[58]	SPWM	*V/f* control	FLC	Matlab/Simulink	0.6
				DSP	1.27
			Modify FLC	Matlab/Simulink	0.593
				DSP	1.12
[146]	SVPWM three level inverter	DFOC	FLC	Matlab/Simulink	2.2
[145]	SVPWM	DTC	FLC	Matlab/Simulink	0.095
				dSPACE	1.5
[178]	SVPWM	IFOC	PI	Matlab/Simulink	0.42
			FLC-PI		0.4
[138]	SPWM	IFOC	FLC-PI	Matlab/Simulink	1.1
				dSPACE	1.57
[4]	SVPWM	*V/f* control	ANN	DSP	2.2
[179]	SPWM	IFOC	PID	Matlab/Simulink	0.3
[115]	SPWM	IFOC	FLC	Matlab/Simulink	0.408
	SPWM	IFOC	FLC	Matlab/Simulink	1.1
[149]	HBPWM	IFOC	ANFIS	Matlab/Simulink	0.075
				dSPACE	1.35
[180]	SPWM	IFOC	FLC	Matlab/Simulink	0.7
				DSP	1
[181]	SPWM	*V/f* control	PI-FLC	Matlab/Simulink	0.17
			PD-FLC	Matlab/Simulink	0.2
			PID-FLC	Matlab/Simulink	0.165
[182]	HBPWM	DTC	PI	Matlab/Simulink	0.591
				dSPACE	2.5
			FLC	Matlab/Simulink	0.531
				dSPACE	2
			Type 2 FLC	Matlab/Simulink	0.478
				dSPACE	1.85
[183]	SPWM	IFOC	FLC	Matlab/Simulink	1.25

microcontroller, dSPACE, FPGA and DSP in application systems.

Table 8 illustrates a comparison on the performance of controllers in TIM in terms of PWM switching techniques, control systems, controller techniques, digital integrated circuits, and settling time for speed response.

VI. ISSUES AND LIMITATIONS

The switching techniques and controller play an important role to enhance the performance for TIM. However, there are some issues and challenges which need to be addressed for the further improvement in performance of TIM.

A. COMPLEX COMPUTATION

The performance of SVPWM switching method is satisfactory because of its minor switching losses and its capability to reduce the harmonics in the output signals. Nonetheless, the SVPWM requires complex calculation in online operation which is the major concern for the real-time

implementation [15], [47], [171]. This limitation could be addressed by employing an ANN and ANFIS based [112], [122] SVPWM, which are considered as the efficient for the inverter operation. Nevertheless, the above-mentioned approaches need a lot of data and a long time for training and learning the linear and nonlinear equations which cause trouble in real-time application.

B. CONVENTIONAL CONTROLLER ISSUES

The conventional controller issues are difficult to obtain on the suitable parameters for conventional performance for TIM control. Also, The conventional controller requires mathematical modeling which is very sensitive to parameter value fluctuation, rapid variation in reference speed, change in temperature, and load disturbances [83], [181], [184].

C. FUZZY LOGIC CONTROLLER ISSUES

The number of MFs and rules are selected based on trial and error approach in the conventional FLC structure. However, this method requires a lot of computation and time until the favorable solution is achieved. Therefore, an adaptive FLC technique is proposed for controlling the speed of an induction motor based on optimization technique. This advanced technique has saved time and reduced the exhaustive trial-and-error process for achieving suitable MFs. The speed controller has been modeled based on appropriate MFs as input and validation results of the objective function computed by the optimization strategy as output.

D. PROTOTYPE IMPLEMENTATION

Many researchers have discussed the hardware implementation of the TIM drive controller using dSPACE, FPGA, and DSP [22], [155], [185]. However, dSPACE and FPGA are very expensive to implement and are not applicable for standalone operation. Moreover, they must be connected to the computer all the time. As for the DSP, it is used in many applications because of its fast computation, low power consumption, short design cycle, embedded processor, and higher density in comparison with other processors. Many existing studies use the specific motor controller to regulate the speed and load of the TIM. Accordingly, a multi-chip controller is needed for the control system of a multi-induction motor drive, but such controller is considered costly.

VII. CONCLUSION AND RECOMMENDATIONS

TIM is the highest energy consumer in the industry and could contribute to energy conservation to save energy cost and reduce the peak power demand. A significant amount of energy can be saved if the speed of the motor can be adjusted with the load. The speed of the motor can be controlled by developing appropriate controllers and switching techniques. The main contribution of this study is the comprehensive explanation of each method of switching techniques, conventional and intelligent controllers and digital integrated circuits including switching pattern, switching time, controller algorithm and mathematical expression, benefits and drawbacks. The methods are discussed and analyzed in a comparative manner, with concrete results.

PWM switching techniques used in the TIM inverter include SPWM, SVPWM, carrier-based PWM, selective harmonic elimination PWM, and HBPWM. Among these techniques, the SVPWM is the best approach for switching and controlling the inverter because it can minimize switching losses and harmonic output signals. The speed of the motor is controlled using two main control strategies, namely, scalar and vector controls. The scalar control method is used in common by researchers due to its simple structure, design and low cost. Besides, this technique can efficiently control the variable speed without considering parameters oh TIM. The vector control method is also commonly used because of its high performance in controlling TIM. The conventional controller has a simple structure, easy design, need mathematical equations and do not need a learning step. On the contrary, intelligent controllers have a complex structure, do not require a mathematical model, and need a learning step and big data to train. Moreover, intelligent controllers achieve good performance if suitable data training, the number of nodes and type of activation functions are selected.

This review has proposed some significant and selective suggestions for the further technological development of TIM controller and switching method, such as:

i. Further investigation should be performed on FLC, ANN and ANFIS based SVPWM switching technique for different configuration of the inverter to improve the accuracy of ANN, ANFIS, and FLC. The intelligent controller such as ANN, ANFIS, and FLC controllers are suggested to implement in TIM to reduce overshoot, settling time, and steady state error.
ii. The performance of ANFIS and FLC can be improved by selecting the appropriate membership function and rules. Also, The ANN accuracy can be enhanced by choosing suitable hidden layer neurons.
iii. Various optimization techniques such as lighting search algorithm, backtracking search algorithm, particle swarm optimization, the genetic algorithm could be used for finding the optimal values and minimum error of ANN, ANFIS, and FLC.
iv. The vector control with DTC, IFOC should be further studied for controlling the position of the flux, voltage, current vectors and minimizing the torque ripple for an induction machine.
v. Further research should be conducted on dSPACE, FPGA, DSP based AI controller.
vi. The research on finding the appropriate value of PID control parameters (K_p, K_i, K_d) should be explored.
vii. The developed controller can be implemented on multi DC motor or multi permanent magnet synchronous motor drive to reduce the manufacturing price of the control system.

These recommendations would be a significant contribution towards the development and implementation of

switching techniques and controllers and would provide a concrete idea for researchers and manufacturers on advancement for future development of TIM.

REFERENCES

[1] S.-M. Lu, "A review of high-efficiency motors: Specification, policy, and technology," *Renew. Sustain. Energy Rev.*, vol. 59, pp. 1–12, Jun. 2016.
[2] A. T. de Almeida, J. Fong, H. Falkner, and P. Bertoldi, "Policy options to promote energy efficient electric motors and drives in the EU," *Renew. Sustain. Energy Rev.*, vol. 74, pp. 1275–1286, Jul. 2017.
[3] I. M. Alsofyani and N. R. N. Idris, "A review on sensorless techniques for sustainable reliablity and efficient variable frequency drives of induction motors," *Renew. Sustain. Energy Rev.*, vol. 24, pp. 111–121, Aug. 2013.
[4] T. H. dos Santos, A. Goedtel, S. A. O. da Silva, and M. Suetake, "Scalar control of an induction motor using a neural sensorless technique," *Electr. Power Syst. Res.*, vol. 108, pp. 322–330, Mar. 2014.
[5] S. A. R. Kashif, M. A. Saqib, and S. Zia, "Implementing the induction-motor drive with four-switch inverter: An application of neural networks," *Expert Syst. Appl.*, vol. 38, no. 9, pp. 11137–11148, Sep. 2011.
[6] R. Saidur, S. Mekhilef, M. B. Ali, A. Safari, and H. A. Mohammed, "Applications of variable speed drive (VSD) in electrical motors energy savings," *Renew. Sustain. Energy Rev.*, vol. 16, no. 1, pp. 543–550, Jan. 2012.
[7] C. M. F. S. Reza, M. D. Islam, and S. Mekhilef, "A review of reliable and energy efficient direct torque controlled induction motor drives," *Renew. Sustain. Energy Rev.*, vol. 37, pp. 919–932, Sep. 2014.
[8] R. Saidur, "A review on electrical motors energy use and energy savings," *Renew. Sustain. Energy Rev.*, vol. 14, no. 3, pp. 877–898, Apr. 2010.
[9] M. S. H. Lipu and T. F. Karim, "Energy efficiency opportunities and savings potential for electric motor and its impact on GHG emissions reduction," *Int. J. Elect. Comput. Eng.*, vol. 3, no. 4, pp. 533–542, Jul. 2013.
[10] M. A. Hannan, J. A. Ali, A. Mohamed, and A. Hussain, "Optimization techniques to enhance the performance of induction motor drives: A review," *Renew. Sustain. Energy Rev.*, vol. 81, no. 2, pp. 1611–1626, Jun. 2017.
[11] M. Jannati *et al.*, "A review on variable speed control techniques for efficient control of single-phase induction motors: Evolution, classification, comparison," *Renew. Sustain. Energy Rev.*, vol. 75, pp. 1306–1319, Aug. 2017.
[12] N. Saad and M. Arrofiq, "A PLC-based modified-fuzzy controller for PWM-driven induction motor drive with constant V/Hz ratio control," *Robot. Comput.-Integr. Manuf.*, vol. 28, no. 2, pp. 95–112, Apr. 2012.
[13] L. Saribulut, A. Teke, and M. Tümay, "Vector-based reference location estimating for space vector modulation technique," *Electr. Power Syst. Res.*, vol. 86, pp. 51–60, May 2012.
[14] G. Durgasukumar and M. K. Pathak, "Comparison of adaptive neuro-fuzzy-based space-vector modulation for two-level inverter," *Int. J. Electr. Power Energy Syst.*, vol. 38, no. 1, pp. 9–19, Jun. 2012.
[15] P. Agarwal, N. Langer, and A. H. Bhat, "Neural-network-based space-vector pulse-width modulation for capacitor voltage balancing of three-phase three-level improved power quality converter," *IET Power Electron.*, vol. 7, no. 4, pp. 973–983, Apr. 2014.
[16] H. Sathishkumar and S. S. Parthasarathy, "A novel neural network intelligent controller for vector controlled induction motor drive," *Energy Procedia*, vol. 138, pp. 692–697, Oct. 2017.
[17] S. Mahapatra, R. Daniel, D. N. Dey, and S. K. Nayak, "Induction motor control using PSO-ANFIS," *Procedia Comput. Sci.*, vol. 48, pp. 753–768, Jan. 2015.
[18] C. Lindner, S. Thiagarajah, J. M. Wilkinson, T. A. Consortium, G. A. Wallis, and T. F. Cootes, "Fully automatic segmentation of the proximal femur using random forest regression voting," *IEEE Trans. Med. Imag.*, vol. 32, no. 8, pp. 1462–1472, Aug. 2013.
[19] J. C. Quiroz, N. Mariun, M. R. Mehrjou, M. Izadi, N. Misron, and M. A. M. Radzi, "Fault detection of broken rotor bar in LS-PMSM using random forests," *Measurement*, vol. 116, pp. 273–280, Feb. 2018.
[20] C. Liu, R. Ma, H. Bai, F. Gechter, and F. Gao, "A new approach for FPGA-based real-time simulation of power electronic system with no simulation latency in subsystem partitioning," *Int. J. Electr. Power Energy Syst.*, vol. 99, pp. 650–658, Jul. 2018.
[21] A. Hazzab, I. K. Bousserhane, M. Zerbo, and P. Sicard, "Real time implementation of fuzzy gain scheduling of PI controller for induction machine control," in *Proc. 2nd Int. Conf. Inf. Commun. Technol.*, vol. 1, Apr. 2006, pp. 1416–1421.
[22] N. Altin and İ. Sefa, "dSPACE based adaptive neuro-fuzzy controller of grid interactive inverter," *Energy Convers. Manage.*, vol. 56, pp. 130–139, Apr. 2012.
[23] K. Premkumar and B. V. Manikandan, "Speed control of brushless DC motor using bat algorithm optimized adaptive neuro-fuzzy inference system," *Appl. Soft Comput.*, vol. 32, pp. 403–419, Jul. 2015.
[24] S. Gdaim, A. Mtibaa, and M. F. Mimouni, "Design and experimental implementation of DTC of an induction machine based on fuzzy logic control on FPGA," *IEEE Trans. Fuzzy Syst.*, vol. 23, no. 3, pp. 644–655, Jun. 2015.
[25] T.-F. Chan and K. Shi, *Applied Intelligent Control of Induction Motor Drives*. Hoboken, NJ, USA: Wiley, 2011.
[26] A. Trzynadlowski, *Control of Induction Motors*. New York, NY, USA: Academic, 2001.
[27] B. M. Wilamowski and J. D. Irwin, *Power Electronics and Motor Drives*. Boca Raton, FL, USA: CRC Press, 2011.
[28] A. Djoudi, S. Bacha, H. Iman-Eini, and T. Rekioua, "Sliding mode control of DFIG powers in the case of unknown flux and rotor currents with reduced switching frequency," *Int. J. Electr. Power Energy Syst.*, vol. 96, pp. 347–356, Mar. 2018.
[29] M. Barnes, *Practical Variable Speed Drives and Power Electronics*. Oxford, U.K.: Newnes, 2003.
[30] A. Singh, B. Grant, R. DeFour, C. Sharma, and S. Bahadoorsingh, "A review of induction motor fault modeling," *Electr. Power Syst. Res.*, vol. 133, pp. 191–197, Apr. 2016.
[31] P. C. Krause, O. Wasynczuk, S. D. Sudhoff, and S. Pekarek, *Analysis of Electric Machinery and Drive Systems*. Piscataway, NJ, USA: IEEE, 2013.
[32] F. H. Gandoman *et al.*, "Review of FACTS technologies and applications for power quality in smart grids with renewable energy systems," *Renew. Sustain. Energy Rev.*, vol. 82, pp. 502–514, Feb. 2018.
[33] H. Abu-Rub, A. Iqbal, and J. Guzinski, *High Performance Control of AC Drives With Matlab/Simulink Models*. Hoboken, NJ, USA: Wiley, 2012.
[34] J. Talla, V. Q. Leu, V. Šmídl, and Z. Peroutka, "Adaptive speed control of induction motor drive with inaccurate model," *IEEE Trans. Ind. Electron.*, vol. 65, no. 11, pp. 8532–8542, Nov. 2018.
[35] M. A. Hannan *et al.*, "A quantum lightning search algorithm-based fuzzy speed controller for induction motor drive," *IEEE Access*, vol. 6, pp. 1214–1223, 2018.
[36] G. Zhang, Z. Li, B. Zhang, and W. A. Halang, "Power electronics converters: Past, present and future," *Renew. Sustain. Energy Rev.*, vol. 81, pp. 2028–2044, Apr. 2018.
[37] N. Mohan, T. M. Undeland, and W. P. Robbins, *Power Electronics: Converters, Applications, and Design*. Hoboken, NJ, USA: Wiley, 2003.
[38] M. Gaballah and M. El-Bardini, "Low cost digital signal generation for driving space vector PWM inverter," *Ain Shams Eng. J.*, vol. 4, no. 4, pp. 763–774, Dec. 2013.
[39] M. A. Hannan, J. A. Ali, A. Mohamed, U. A. U. Amirulddin, N. M. L. Tan, and M. N. Uddin, "Quantum-behaved lightning search algorithm to improve indirect field-oriented fuzzy-PI control for IM drive," in *Proc. IEEE Ind. Appl. Soc. Annu. Meeting*, Mar. 2017, pp. 1–8.
[40] B. K. Bose, "Scalar decoupled control of induction motor," *IEEE Trans. Ind. Appl.*, vol. IA-20, no. 1, pp. 216–225, Jan. 1984.
[41] W. Liang, J. Wang, P. C.-K. Luk, W. Fang, and W. Fei, "Analytical modeling of current harmonic components in PMSM drive with voltage-source inverter by SVPWM technique," *IEEE Trans. Energy Convers.*, vol. 29, no. 3, pp. 673–680, Sep. 2014.
[42] X. Zhang, W. Zhang, J. Chen, and D. Xu, "Deadbeat control strategy of circulating currents in parallel connection system of three-phase PWM converter," *IEEE Trans. Energy Convers.*, vol. 29, no. 2, pp. 406–417, Jun. 2014.
[43] H. Guzman, F. Barrero, and M. J. Duran, "IGBT-gating failure effect on a fault-tolerant predictive current-controlled five-phase induction motor drive," *IEEE Trans. Ind. Electron.*, vol. 62, no. 1, pp. 15–20, Jan. 2015.
[44] E. Velander, L. Kruse, T. L. Wiik, A. Wiberg, J. Colmenares, and H.-P. Nee, "An IGBT turn-ON concept offering low losses under motor drive dv/dt constraints based on diode current adaption," *IEEE Trans. Power Electron.*, vol. 33, no. 2, pp. 1143–1153, Feb. 2018.

[45] M. Amiri, J. Milimonfared, and D. A. Khaburi, "Predictive torque control implementation for induction motors based on discrete space vector modulation," *IEEE Trans. Ind. Electron.*, vol. 65, no. 9, pp. 6881–6889, Sep. 2018.

[46] M. Boby, K. Gopakumar, L. Umanand, F. Blaabjerg, and S. Bhattacharya, "A low-order harmonic elimination scheme for induction motor drives using a multilevel octadecagonal space vector structure with a single DC source," *IEEE Trans. Power Electron.*, vol. 33, no. 3, pp. 2430–2437, Mar. 2018.

[47] B. Kirankumar, Y. V. S. Reddy, and M. Vijayakumar, "Multilevel inverter with space vector modulation: Intelligence direct torque control of induction motor," *IET Power Electron.*, vol. 10, no. 10, pp. 1129–1137, Aug. 2017.

[48] A. Munoz-Garcia, T. A. Lipo, and D. W. Novotny, "A new induction motor V/f control method capable of high-performance regulation at low speeds," *IEEE Trans. Ind. Appl.*, vol. 34, no. 4, pp. 813–821, Jul. 1998.

[49] S. F. Rabbi, M. Halloran, T. LeDrew, A. Matchem, and M. A. Rahman, "Modeling and V/f control of a hysteresis interior permanent-magnet motor," *IEEE Trans. Ind. Appl.*, vol. 52, no. 2, pp. 1891–1901, Mar. 2016.

[50] M. S. Boroujeni, G. A. Markadeh, J. Soltani, and F. Blaabjerg, "Torque ripple reduction of brushless DC motor with harmonic current injection based on integral terminal sliding mode control," *IET Electr. Power Appl.*, vol. 12, no. 1, pp. 25–36, Jan. 2018.

[51] C. Yang, T. Ma, Z. Che, and L. Zhou, "An adaptive-gain sliding mode observer for sensorless control of permanent magnet linear synchronous motors," *IEEE Access*, vol. 6, pp. 3469–3478, 2018.

[52] R. Ancuti, I. Boldea, and G.-D. Andreescu, "Sensorless V/f control of high-speed surface permanent magnet synchronous motor drives with two novel stabilising loops for fast dynamics and robustness," *IET Electr. Power Appl.*, vol. 4, no. 3, pp. 149–157, 2010.

[53] A. B. de Souza Júnior, E. C. de Diniz, D. A. de Honorio, L. H. S. C. Barreto, and L. L. N. dos Reis, "Hybrid control robust using logic fuzzy applied to the position loop for vector control to induction motors," *Electr. Power Compon. Syst.*, vol. 42, no. 6, pp. 533–543, Apr. 2014.

[54] T. Sutikno, N. R. N. Idris, and A. Jidin, "A review of direct torque control of induction motors for sustainable reliability and energy efficient drives," *Renew. Sustain. Energy Rev.*, vol. 32, pp. 548–558, Apr. 2014.

[55] Z. Dong, Y. Yu, W. Li, B. Wang, and D. Xu, "Flux-weakening control for induction motor in voltage extension region: Torque analysis and dynamic performance improvement," *IEEE Trans. Ind. Electron.*, vol. 65, no. 5, pp. 3740–3751, May 2018.

[56] S. Maiti, V. Verma, C. Chakraborty, and Y. Hori, "An adaptive speed sensorless induction motor drive with artificial neural network for stability enhancement," *IEEE Trans. Ind. Informat.*, vol. 8, no. 4, pp. 757–766, Nov. 2012.

[57] A. Tripathi and G. Narayanan, "Torque ripple minimization in neutral-point-clamped three-level inverter fed induction motor drives operated at low-switching-frequency," *IEEE Trans. Ind. Appl.*, vol. 54, no. 3, pp. 2370–2380, May 2018.

[58] H.-S. Jung, C.-E. Hwang, H.-S. Kim, S.-K. Sul, H.-W. An, and H. Yoo, "Minimum torque ripple pulse width modulation with reduced switching frequency for medium-voltage motor drive," *IEEE Trans. Ind. Appl.*, vol. 54, no. 4, pp. 3315–3325, Jul./Aug. 2018.

[59] A. Smith, S. Gadoue, M. Armstrong, and J. Finch, "Improved method for the scalar control of induction motor drives," *IET Electr. Power Appl.*, vol. 7, no. 6, pp. 487–498, Jul. 2013.

[60] S.-C. Agarlita, C.-E. Coman, G.-D. Andreescu, and I. Boldea, "Stable V/f control system with controlled power factor angle for permanent magnet synchronous motor drives," *IET Electr. Power Appl.*, vol. 7, no. 4, pp. 278–286, Apr. 2013.

[61] D. Zhou, Y. Li, J. Zhao, F. Wu, and H. Luo, "An embedded closed-loop fault-tolerant control scheme for nonredundant VSI-fed induction motor drives," *IEEE Trans. Power Electron.*, vol. 32, no. 5, pp. 3731–3740, May 2017.

[62] M. Suetake, I. N. da Silva, and A. Goedtel, "Embedded DSP-based compact fuzzy system and its application for induction-motor V/f speed control," *IEEE Trans. Ind. Electron.*, vol. 58, no. 3, pp. 750–760, Mar. 2011.

[63] R. A. V. Eck, "The separately excited DC traction motor applied to DC and single-phase AC rapid transit systems and electrified railroads, Part I," *IEEE Trans. Ind. General Appl.*, vol. IGA-7, no. 5, pp. 643–649, Sep. 1971.

[64] C. Jiang, K. T. Chau, T. W. Ching, C. Liu, and W. Han, "Time-division multiplexing wireless power transfer for separately excited DC motor drives," *IEEE Trans. Magn.*, vol. 53, no. 11, Nov. 2017, Art. no. 8205405.

[65] R. Hedjar, P. Boucher, and D. Dumur, "Robust nonlinear receding-horizon control of induction motors," *Int. J. Electr. Power Energy Syst.*, vol. 46, pp. 353–365, Mar. 2013.

[66] O. Barambones and P. Alkorta, "A robust vector control for induction motor drives with an adaptive sliding-mode control law," *J. Franklin Inst.*, vol. 348, no. 2, pp. 300–314, Mar. 2011.

[67] B. K. Bose, *Modern Power Electronics and AC Drives*. Upper Saddle River, NJ, USA: Prentice-Hall, 2002.

[68] C. B. Butt and M. A. Rahman, "Intelligent speed control of interior permanent magnet motor drives using a single untrained artificial neuron," *IEEE Trans. Ind. Appl.*, vol. 49, no. 4, pp. 1836–1843, Jul. 2013.

[69] F. F. M. El-Sousy, "Robust wavelet-neural-network sliding-mode control system for permanent magnet synchronous motor drive," *IET Electr. Power Appl.*, vol. 5, no. 1, pp. 113–132, 2011.

[70] A. A. S. Mohamed, A. Berzoy, and O. A. Mohammed, "Design and hardware implementation of FL-MPPT control of PV systems based on GA and small-signal analysis," *IEEE Trans. Sustain. Energy*, vol. 8, no. 1, pp. 279–290, Jan. 2017.

[71] S. Bennett, "Nicholas minorsky and the automatic steering of ships," *IEEE Control Syst. Mag.*, vol. 4, no. 4, pp. 10–15, Nov. 1984.

[72] R. Francis and I. A. Chidambaram, "Optimized PI+ load–frequency controller using BWNN approach for an interconnected reheat power system with RFB and hydrogen electrolyser units," *Int. J. Electr. Power Energy Syst.*, vol. 67, pp. 381–392, May 2015.

[73] X. Luan, Q. Chen, and F. Liu, "Centralized PI control for high dimensional multivariable systems based on equivalent transfer function," *ISA Trans.*, vol. 53, no. 5, pp. 1554–1561, Sep. 2014.

[74] H. H. Choi, H. M. Yun, and Y. Kim, "Implementation of evolutionary fuzzy PID speed controller for PM synchronous motor," *IEEE Trans. Ind. Informat.*, vol. 11, no. 2, pp. 540–547, Apr. 2015.

[75] S. Lekhchine, T. Bahi, and Y. Soufi, "Indirect rotor field oriented control based on fuzzy logic controlled double star induction machine," *Int. J. Electr. Power Energy Syst.*, vol. 57, pp. 206–211, May 2014.

[76] H. Li, "Tuning of PI–PD controller using extended non-minimal state space model predictive control for the stabilized gasoline vapor pressure in a stabilized tower," *Chemometrics Intell. Lab. Syst.*, vol. 142, pp. 1–8, Mar. 2015.

[77] P. D. Ngo and Y. C. Shin, "Gain estimation of nonlinear dynamic systems modeled by an FBFN and the maximum output scaling factor of a self-tuning PI fuzzy controller," *Eng. Appl. Artif. Intell.*, vol. 42, pp. 1–15, Jun. 2015.

[78] J. Zhong and L. Li, "Tuning fractional-order $PI^{\lambda}D^{\mu}$ controllers for a solid-core magnetic bearing system," *IEEE Trans. Control Syst. Technol.*, vol. 23, no. 4, pp. 1648–1656, Jul. 2015.

[79] A. G. Daful, "Comparative study of PID tuning methods for processes with large & small delay times," in *Proc. Adv. Sci. Eng. Technol. Int. Conf. (ASET)*, Feb. 2018, pp. 1–7.

[80] M. M. Hoque, M. A. Hannan, and A. Mohamed, "Charging and discharging model of lithium-ion battery for charge equalization control using particle swarm optimization algorithm," *J. Renew. Sustain. Energy*, vol. 8, no. 6, p. 065701, Nov. 2016.

[81] S. Hazra and P. S. Sensarma, "Self-excitation and control of an induction generator in a stand-alone wind energy conversion system," *IET Renew. Power Gener.*, vol. 4, no. 4, pp. 383–393, 2010.

[82] S. Demirbas, "Self-tuning fuzzy-PI-based current control algorithm for doubly fed induction generator," *IET Renew. Power Gener.*, vol. 11, no. 13, pp. 1714–1722, Nov. 2017.

[83] A. L. L. F. Murari *et al.*, "A proposal of project of PI controller gains used on the control of doubly-fed induction generators," *IEEE Latin Amer. Trans.*, vol. 15, no. 2, pp. 173–180, Feb. 2017.

[84] H. B. Azza, M. Jemli, M. Boussak, and M. Gossa, "High performance sensorless speed vector control of SPIM drives with on-line stator resistance estimation," *Simul. Model. Pract. Theory*, vol. 19, no. 1, pp. 271–282, Jan. 2011.

[85] D. A. Dominic and T. R. Chelliah, "Analysis of field-oriented controlled induction motor drives under sensor faults and an overview of sensorless schemes," *ISA Trans.*, vol. 53, no. 5, pp. 1680–1694, Sep. 2014.

[86] M. Arrouf and N. Bouguechal, "Vector control of an induction motor fed by a photovoltaic generator," *Appl. Energy*, vol. 74, nos. 1–2, pp. 159–167, Jan. 2003.

[87] M. S. Zaky and M. K. Metwaly, "A performance investigation of a four-switch three-phase inverter-fed IM drives at low speeds using fuzzy logic and PI controllers," *IEEE Trans. Power Electron.*, vol. 32, no. 5, pp. 3741–3753, May 2017.
[88] R. H. Kumar, A. Iqbal, and N. C. Lenin, "Review of recent advancements of direct torque control in induction motor drives—A decade of progress," *IET Power Electron.*, vol. 11, no. 1, pp. 1–15, Jan. 2018.
[89] M. H. Holakooie, M. Ojaghi, and A. Taheri, "Direct torque control of six-phase induction motor with a novel MRAS-based stator resistance estimator," *IEEE Trans. Ind. Electron.*, vol. 65, no. 10, pp. 7685–7696, Oct. 2018.
[90] M. Manohar and S. Das, "Current sensor fault-tolerant control for direct torque control of induction motor drive using flux-linkage observer," *IEEE Trans. Ind. Informat.*, vol. 13, no. 6, pp. 2824–2833, Dec. 2017.
[91] M. S. H. Lipu, M. A. Hannan, A. Hussain, M. H. M. Saad, A. Ayob, and F. Blaabjerg, "State of charge estimation for lithium-ion battery using recurrent NARX neural network model based lighting search algorithm," *IEEE Access*, vol. 6, pp. 28150–28161, 2018.
[92] M. S. H. Lipu, M. A. Hannan, A. Hussain, and M. H. M. Saad, "Optimal BP neural network algorithm for state of charge estimation of lithium-ion battery using PSO with PCA feature selection," *J. Renew. Sustain. Energy*, vol. 9, no. 6, p. 064102, Nov. 2017.
[93] M. A. Hannan, M. S. H. Lipu, A. Hussain, M. H. Saad, and A. Ayob, "Neural network approach for estimating state of charge of lithium-ion battery using backtracking search algorithm," *IEEE Access*, vol. 6, pp. 10069–10079, 2018.
[94] M. S. H. Lipu, A. Hussain, M. H. M. Saad, and M. A. Hannan, "Optimal neural network approach for estimating state of energy of lithium-ion battery using heuristic optimization techniques," in *Proc. 6th Int. Conf. Elect. Eng. Inform. (ICEEI)*, Nov. 2017, pp. 1–6.
[95] M. S. H. Lipu, A. Hussain, M. H. M. Saad, A. Ayob, and M. A. Hannan, "Improved recurrent NARX neural network model for state of charge estimation of lithium-ion battery using pso algorithm," in *Proc. IEEE Symp. Comput. Appl. Ind. Electron. (ISCAIE)*, Apr. 2018, pp. 354–359.
[96] L. Guo and L. Parsa, "Model reference adaptive control of five-phase IPM motors based on neural network," *IEEE Trans. Ind. Electron.*, vol. 59, no. 3, pp. 1500–1508, Mar. 2012.
[97] C.-M. Hong, F.-S. Cheng, and C.-H. Chen, "Optimal control for variable-speed wind generation systems using general regression neural network," *Int. J. Electr. Power Energy Syst.*, vol. 60, pp. 14–23, Sep. 2014.
[98] Y. Oguz and M. Dede, "Speed estimation of vector controlled squirrel cage asynchronous motor with artificial neural networks," *Energy Convers. Manage.*, vol. 52, no. 1, pp. 675–686, Jan. 2011.
[99] C.-K. Lin, "Radial basis function neural network-based adaptive critic control of induction motors," *Appl. Soft Comput.*, vol. 11, no. 3, pp. 3066–3074, Apr. 2011.
[100] N. Lashkari, J. Poshtan, and H. F. Azgomi, "Simulative and experimental investigation on stator winding turn and unbalanced supply voltage fault diagnosis in induction motors using artificial neural networks," *ISA Trans.*, vol. 59, pp. 334–342, Nov. 2015.
[101] A. Y. Alanis, J. D. Rios, J. Rivera, N. Arana-Daniel, and C. Lopez-Franco, "Real-time discrete neural control applied to a linear induction motor," *Neurocomputing*, vol. 164, pp. 240–251, Sep. 2015.
[102] R. H. C. Palácios, I. N. da Silva, A. Goedtel, and W. F. Godoy, "A comprehensive evaluation of intelligent classifiers for fault identification in three-phase induction motors," *Electr. Power Syst. Res.*, vol. 127, pp. 249–258, Oct. 2015.
[103] C. T. Krasopoulos, M. E. Beniakar, and A. G. Kladas, "Multicriteria PM motor design based on ANFIS evaluation of EV driving cycle efficiency," *IEEE Trans. Transport. Electrific.* , vol. 4, no. 2, pp. 525–535, Jun. 2018.
[104] H. Yang, Y. Fu, and D. Wang, "Multi-ANFIS model based synchronous tracking control of high-speed electric multiple unit," *IEEE Trans. Fuzzy Syst.*, vol. 26, no. 3, pp. 1472–1484, Jun. 2018.
[105] X. Tian, R. He, and Y. Xu, "Design of an energy management strategy for a parallel hybrid electric bus based on an IDP-ANFIS scheme," *IEEE Access*, vol. 6, pp. 23806–23819, 2018.
[106] M. A. Hannan, M. S. H. Lipu, A. Hussain, and A. Mohamed, "A review of lithium-ion battery state of charge estimation and management system in electric vehicle applications: Challenges and recommendations," *Renew. Sustain. Energy Rev.*, vol. 78, pp. 834–854, Oct. 2017.
[107] A. Senthilkumar and P. Ajay-D-Vimal Raj, "ANFIS and MRAS-PI controllers based adaptive-UPQC for power quality enhancement application," *Electr. Power Syst. Res.*, vol. 126, pp. 1–11, Sep. 2015.
[108] F. Liu, H. Wang, Q. Shi, H. Wang, M. Zhang, and H. Zhao, "Comparison of an ANFIS and fuzzy PID control model for performance in a two-axis inertial stabilized platform," *IEEE Access*, vol. 5, pp. 12951–12962, 2017.
[109] F. G. Areed, A. Y. Haikal, and R. H. Mohammed, "Adaptive neuro-fuzzy control of an induction motor," *Ain Shams Eng. J.*, vol. 1, no. 1, pp. 71–78, Sep. 2010.
[110] P. Subbaraj and B. Kannapiran, "Fault detection and diagnosis of pneumatic valve using adaptive neuro-fuzzy inference system approach," *Appl. Soft Comput.*, vol. 19, pp. 362–371, Jun. 2014.
[111] F. Lima, W. Kaiser, I. N. da Silva, and A. A. de Oliveira, "Speed neuro-fuzzy estimator applied to sensorless induction motor control," *IEEE Latin Amer. Trans.*, vol. 10, no. 5, pp. 2065–2073, Sep. 2012.
[112] F. Lima, W. Kaiser, I. N. da Silva, and A. A. A. de Oliveira, Jr., "Open-loop neuro-fuzzy speed estimator applied to vector and scalar induction motor drives," *Appl. Soft Comput.*, vol. 21, pp. 469–480, Aug. 2014.
[113] M. N. Uddin, "An adaptive-filter-based torque-ripple minimization of a fuzzy-logic controller for speed control of IPM motor drives," *IEEE Trans. Ind. Appl.*, vol. 47, no. 1, pp. 350–358, Jan. 2011.
[114] P.-C. Cheng, B.-R. Peng, Y.-H. Liu, Y.-S. Cheng, and J.-W. Huang, "Optimization of a fuzzy-logic-control-based MPPT algorithm using the particle swarm optimization technique," *Energies*, vol. 8, no. 6, pp. 5338–5360, Jun. 2015.
[115] S. Rafa, A. Larabi, L. Barazane, M. Manceur, N. Essounbouli, and A. Hamzaoui, "Implementation of a new fuzzy vector control of induction motor," *ISA Trans.*, vol. 53, no. 3, pp. 744–754, May 2014.
[116] M. Uddin and M. Hafeez, "FLC-based DTC scheme to improve the dynamic performance of an IM drive," *IEEE Trans. Ind. Appl.*, vol. 48, no. 2, pp. 823–831, Mar. 2012.
[117] X.-D. Sun, K.-H. Koh, B.-G. Yu, and M. Matsui, "Fuzzy-logic-based V/f control of an induction motor for a DC grid power-leveling system using flywheel energy storage equipment," *IEEE Trans. Ind. Electron.*, vol. 56, no. 8, pp. 3161–3168, Aug. 2009.
[118] C.-L. Chiang and C.-T. Su, "Tracking control of induction motor using fuzzy phase plane controller with improved genetic algorithm," *Electr. Power Syst. Res.*, vol. 73, no. 2, pp. 239–247, Feb. 2005.
[119] O. Yazdanbakhsh and S. Dick, "A systematic review of complex fuzzy sets and logic," *Fuzzy Sets Syst.*, vol. 338, pp. 1–22, May 2018.
[120] Y.-C. Luo and W.-X. Chen, "Sensorless stator field orientation controlled induction motor drive with a fuzzy speed controller," *Comput. Math. Appl.*, vol. 64, no. 5, pp. 1206–1216, Sep. 2012.
[121] N. Bounar, A. Boulkroune, F. Boudjema, M. M'Saad, and M. Farza, "Adaptive fuzzy vector control for a doubly-fed induction motor," *Neurocomputing*, vol. 151, pp. 756–769, Mar. 2015.
[122] T. G. Nathenas and G. A. Adamidis, "A new approach for SVPWM of a three-level inverter-induction motor fed-neutral point balancing algorithm," in *Proc. Int. Aegean Conf. Elect. Mach. Power Electron. Electromotion*, 2011, pp. 221–226.
[123] A. Verma, S. Sarangi, and M. H. Kolekar, "Stator winding fault prediction of induction motors using multiscale entropy and grey fuzzy optimization methods," *Comput. Electr. Eng.*, vol. 40, no. 7, pp. 2246–2258, Oct. 2014.
[124] S. Chekkal, N. A. Lahaçani, D. Aouzellag, and K. Ghedamsi, "Fuzzy logic control strategy of wind generator based on the dual-stator induction generator," *Int. J. Electr. Power Energy Syst.*, vol. 59, pp. 166–175, Jul. 2014.
[125] M. C. Paicu, I. Boldea, G.-D. Andreescu, and F. Blaabjerg, "Very low speed performance of active flux based sensorless control: Interior permanent magnet synchronous motor vector control versus direct torque and flux control," *IET Electr. Power Appl.*, vol. 3, no. 6, pp. 551–561, 2009.
[126] V. Calderaro, V. Galdi, A. Piccolo, and P. Siano, "A fuzzy controller for maximum energy extraction from variable speed wind power generation systems," *Electr. Power Syst. Res.*, vol. 78, no. 6, pp. 1109–1118, Jun. 2008.
[127] S. Velusami and S. Singaravelu, "Steady state modeling and fuzzy logic based analysis of wind driven single phase induction generators," *Renew. Energy*, vol. 32, no. 14, pp. 2386–2406, Nov. 2007.
[128] Z. M. S. El-Barbary, "Fuzzy logic based controller for five-phase induction motor drive system," *Alexandria Eng. J.*, vol. 51, no. 4, pp. 263–268, Dec. 2012.
[129] S.-Y. Wang, C.-L. Tseng, and C.-J. Chiu, "Design of a novel adaptive TSK-fuzzy speed controller for use in direct torque control induction motor drives," *Appl. Soft Comput.*, vol. 31, pp. 396–404, Jun. 2015.

[130] M. Allouche, M. Souissi, M. Chaabane, and D. Mehdi, "Fuzzy tracking control for indirect field-oriented induction machine using integral action performance," *IETE J. Res.*, vol. 57, no. 5, pp. 443–451, 2011.

[131] H. H. Choi, J.-W. Jung, and R.-Y. Kim, "Fuzzy adaptive speed control of a permanent magnet synchronous motor," *Int. J. Electron.*, vol. 99, no. 5, pp. 657–672, May 2012.

[132] L. Zhan and K. Zhou, "Field-programmable gate array based fuzzy sliding-mode controller for a permanent magnet synchronous motor drive," *Electr. Power Compon. Syst.*, vol. 42, no. 13, pp. 1440–1451, Oct. 2014.

[133] R. Goswami and D. Joshi, "Performance review of fuzzy logic based controllers employed in brushless DC motor," *Procedia Comput. Sci.*, vol. 132, pp. 623–631, Dec. 2018.

[134] Y. Zhang, J. Zhu, Z. Zhao, W. Xu, and D. G. Dorrell, "An improved direct torque control for three-level inverter-fed induction motor sensorless drive," *IEEE Trans. Power Electron.*, vol. 27, no. 3, pp. 1502–1513, Mar. 2012.

[135] S. Ozdemir, O. Kaplan, I. Sefa, and N. Altin, "Fuzzy PI controlled inverter for grid interactive renewable energy systems," *IET Renew. Power Gener.*, vol. 9, no. 7, pp. 729–738, Sep. 2015.

[136] M. N. Uddin, T. S. Radwan, and M. A. Rahman, "Performances of novel fuzzy logic based indirect vector control for induction motor drive," in *Proc. Conf. Rec. IEEE Ind. Appl. 35th IAS Annu. Meeting World Conf. Ind. Appl. Elect. Energy*, vol. 2, Oct. 2000, pp. 1225–1231.

[137] M. Masiala, B. Vafakhah, J. Salmon, and A. Knight, "Fuzzy self-tuning speed control of an indirect field-oriented control induction motor drive," in *Proc. IEEE Ind. Appl. Annu. Meeting*, Sep. 2007, pp. 1008–1014.

[138] A. Lokriti, I. Salhi, S. Doubabi, and Y. Zidani, "Induction motor speed drive improvement using fuzzy IP-self-tuning controller. A real time implementation," *ISA Trans.*, vol. 52, no. 3, pp. 406–417, May 2013.

[139] I. Pan, S. Das, and A. Gupta, "Tuning of an optimal fuzzy PID controller with stochastic algorithms for networked control systems with random time delay," *ISA Trans.*, vol. 50, no. 1, pp. 28–36, Jan. 2011.

[140] R. K. Sahu, S. Panda, and N. K. Yegireddy, "A novel hybrid DEPS optimized fuzzy PI/PID controller for load frequency control of multi-area interconnected power systems," *J. Process Control*, vol. 24, no. 10, pp. 1596–1608, Oct. 2014.

[141] J. Velagic, M. Kuric, E. Dragolj, Z. Ajanovic, and N. Osmic, "Micro-controller based fuzzy-PI approach employing control surface discretization," in *Proc. 20th Medit. Conf. Control Automat. (MED)*, Jul. 2012, pp. 638–645.

[142] K. Belmokhtar, M. L. Doumbia, and K. Agbossou, "Novel fuzzy logic based sensorless maximum power point tracking strategy for wind turbine systems driven DFIG (doubly-fed induction generator)," *Energy*, vol. 76, pp. 679–693, Nov. 2014.

[143] M. Hu, J. Qiu, and C. Shi, "A comparative analysis of fuzzy PI and PI speed control in Brushless DC motor based on dSPACE," in *Proc. Int. Conf. Elect. Mach. Syst.*, Aug. 2011, pp. 1–5.

[144] C. Y. Seng and Z. Ibrahim, "Vector control drive of permanent magnet synchronous motor based dSPACE DS1103 implementation," in *Proc. IEEE Int. Power Eng. Optim. Conf.*, Jun. 2012, pp. 147–152.

[145] X. Li and W. Li, "Design of an dSPACE-based 3-phase SVPWM controller," in *Proc. Int. Conf. Elect. Control Eng.*, Sep. 2011, pp. 2134–2137.

[146] H. Akroum, M. Kidouche, and A. Aibeche, "A dSPACE DSP control platform for V/f controlled induction motor drive and parameters identification," in *Advances in Computer, Communication, Control and Automation*. Berlin, Germany: Springer, 2011, pp. 305–312.

[147] M. Jemli, H. B. Azza, and M. Gossa, "Real-time implementation of IRFOC for single-phase induction motor drive using dSpace DS 1104 control board," *Simul. Model. Pract. Theory*, vol. 17, no. 6, pp. 1071–1080, Jul. 2009.

[148] A. Abbou, Y. Sayouti, H. Mahmoudi, and M. Akherraz, "dSPACE direct torque control implementation for induction motor," in *Proc. 18th Medit. Conf. Control Autom. (MED)*, Jun. 2010, pp. 1121–1126.

[149] M. N. Uddin, Z. R. Huang, and A. B. M. S. Hossain, "Development and implementation of a simplified self-tuned neuro-fuzzy-based IM drive," in *Proc. IEEE Ind. Appl. Soc. Annu. Meeting*, Oct. 2011, pp. 1–7.

[150] A. Guellal, C. Larbes, D. Bendib, L. Hassaine, and A. Malek, "FPGA based on-line artificial neural network selective harmonic elimination PWM technique," *Int. J. Electr. Power Energy Syst.*, vol. 68, pp. 33–43, Jun. 2015.

[151] E. Cabal-Yepez *et al.*, "FPGA-based entropy neural processor for online detection of multiple combined faults on induction motors," *Mech. Syst. Signal Process.*, vol. 30, pp. 123–130, Jul. 2012.

[152] D. Zhang and H. Li, "A stochastic-based FPGA controller for an induction motor drive with integrated neural network algorithms," *IEEE Trans. Ind. Electron.*, vol. 55, no. 2, pp. 551–561, Feb. 2008.

[153] L. M. Contreras-Medina, R. de Jesus Romero-Troncoso, E. Cabal-Yepez, J. de Jesus Rangel-Magdaleno, and J. R. Millan-Almaraz, "FPGA-based multiple-channel vibration analyzer for industrial applications in induction motor failure detection," *IEEE Trans. Instrum. Meas.*, vol. 59, no. 1, pp. 63–72, Jan. 2010.

[154] G. Renukadevi and K. Rajambal, "Field programmable gate array implementation of space-vector pulse-width modulation technique for five-phase voltage source inverter," *IET Power Electron.*, vol. 7, no. 2, pp. 376–389, Feb. 2014.

[155] G. Wang, R. Yang, and D. Xu, "DSP-based control of sensorless IPMSM drives for wide-speed-range operation," *IEEE Trans. Ind. Electron.*, vol. 60, no. 2, pp. 720–727, Feb. 2013.

[156] F. J. Lin, P. H. Chou, C. S. Chen, and Y. S. Lin, "DSP-based cross-coupled synchronous control for dual linear motors via intelligent complementary sliding mode control," *IEEE Trans. Ind. Electron.*, vol. 59, no. 2, pp. 1061–1073, Feb. 2012.

[157] B. H. Sun, "The implication of four-quadrant H-bridge cascaded multi-level inverters in the speed control system of high-voltage motor," in *Proc. Int. Conf. Elect. Control Eng.*, Jun. 2010, pp. 4418–4421.

[158] R. Abdelli, D. Rekioua, and T. Rekioua, "Performances improvements and torque ripple minimization for VSI fed induction machine with direct control torque," *ISA Trans.*, vol. 50, no. 2, pp. 213–219, Apr. 2011.

[159] X. Zhang, X. Xie, and R. Yao, "Field oriented control for permanent magnet synchronous motor based on DSP experimental platform," in *Proc. 27th Chin. Control Decis. Conf. (CCDC)*, May 2015, pp. 1870–1875.

[160] G. Y. Chen and J.-W. Perng, "PI speed controller design based on GA with time delay for BLDC motor using DSP," in *Proc. IEEE Int. Conf. Mechatronics Automat. (ICMA)*, Aug. 2017, pp. 1174–1179.

[161] S. Kumar and A. Deshpande, "DSP based close-loop speed control system for DC motor using dual converter," in *Proc. Annu. IEEE India Conf. (INDICON)*, Dec. 2014, pp. 1–7.

[162] V. Anuja, M. B. J. Ananth, and M. A. Mary, "Three level voltage inverter using synchronized SVPWM and DSP," in *Proc. Int. Conf. Elect., Electron., Optim. Techn. (ICEEOT)*, Mar. 2016, pp. 4748–4753.

[163] F. Zidani, M. S. N. Said, R. Abdessemed, D. Diallo, and M. E. H. Benbouzid, "A fuzzy technique for loss minimization in scalar-controlled induction motor," *Electr. Power Compon. Syst.*, vol. 30, no. 6, pp. 625–635, Jun. 2002.

[164] S. V. Ustun and M. Demirtas, "Optimal tuning of PI coefficients by using fuzzy-genetic for V/f controlled induction motor," *Expert Syst. Appl.*, vol. 34, no. 4, pp. 2714–2720, May 2008.

[165] S. K. Mondal, J. O. P. Pinto, and B. K. Bose, "A neural-network-based space-vector PWM controller for a three-level voltage-fed inverter induction motor drive," *IEEE Trans. Ind. Appl.*, vol. 38, no. 3, pp. 660–669, May 2002.

[166] P. Agarwal, N. Langer, and A. H. Bhat, "Neural-network-based space-vector pulse-width modulation for capacitor voltage balancing of three-phase three-level improved power quality converter," *IET Power Electron.*, vol. 7, no. 4, pp. 973–983, Apr. 2014.

[167] K. M. Woodley, H. Li, and S. Y. Foo, "Neural network modeling of torque estimation and d–q transformation for induction machine," *Eng. Appl. Artif. Intell.*, vol. 18, no. 1, pp. 57–63, Feb. 2005.

[168] R. Verma, V. Verma, and C. Chakraborty, "ANN based sensorless vector controlled induction motor drive suitable for four quadrant operation," in *Proc. IEEE Students Technol. Symp.*, Feb. 2014, pp. 182–187.

[169] M. Demirtas, "DSP-based sliding mode speed control of induction motor using neuro-genetic structure," *Expert Syst. Appl.*, vol. 36, no. 3, pp. 5533–5540, Apr. 2009.

[170] S. V. Ustun and M. Demirtas, "Modeling and control of V/f controlled induction motor using genetic-ANFIS algorithm," *Energy Convers. Manage.*, vol. 50, no. 3, pp. 786–791, Mar. 2009.

[171] A. R. Beig, "Constant V/f induction motor drive with synchronised space vector pulse width modulation," *IET Power Electron.*, vol. 5, no. 8, pp. 1446–1455, 2012.

[172] H. M. Kojabadi, "Simulation and experimental studies of model reference adaptive system for sensorless induction motor drive," *Simul. Model. Pract. Theory*, vol. 13, no. 6, pp. 451–464, Sep. 2005.

[173] M. A. Mannan, T. Murata, J. Tamura, and T. Tsuchiya, "A fuzzy-logic-based self-tuning PI controller for high-performance vector controlled induction motor drive," *Electr. Power Compon. Syst.*, vol. 34, no. 4, pp. 471–481, Apr. 2006.
[174] S.-M. Kim and W.-Y. Han, "Induction motor servo drive using robust PID-like neuro-fuzzy controller," *Control Eng. Pract.*, vol. 14, no. 5, pp. 481–487, May 2006.
[175] M. N. Uddin and H. Wen, "Development of a self-tuned neuro-fuzzy controller for induction motor drives," *IEEE Trans. Ind. Appl.*, vol. 43, no. 4, pp. 1108–1116, Jul. 2007.
[176] S. Barkati, E. M. Berkouk, and M. S. Boucherit, "Application of type-2 fuzzy logic controller to an induction motor drive with seven-level diode-clamped inverter and controlled infeed," *Elect. Eng.*, vol. 90, no. 5, pp. 347–359, May 2008.
[177] S. M. Gadoue, D. Giaouris, and J. W. Finch, "Artificial intelligence-based speed control of DTC induction motor drives—A comparative study," *Electr. Power Syst. Res.*, vol. 79, no. 1, pp. 210–219, Jan. 2009.
[178] Febin Daya J.L., V. Subbiah, and P. Sanjeevikumar, "Robust speed control of an induction motor drive using wavelet-fuzzy based self-tuning multiresolution controller," *Int. J. Comput. Intell. Syst.*, vol. 6, no. 4, pp. 724–738, Aug. 2013.
[179] E. S. Abdin, G. A. Ghoneem, H. M. M. Diab, and S. A. Deraz, "Efficiency optimization of a vector controlled induction motor drive using an artificial neural network," in *Proc. 29th Annu. Conf. IEEE Ind. Electron. Soc.*, vol. 3, Nov. 2003, pp. 2543–2548.
[180] S.-Y. Wang, C.-L. Tseng, C.-Y. Chang, and J.-H. Chou, "Estimator-based fuzzy credit-assigned cerebellar model articulation controller design for vector-controlled induction motor drives," *J. Chin. Inst. Eng.*, vol. 37, no. 3, pp. 332–345, Apr. 2014.
[181] S. Pati, M. Patnaik, and A. Panda, "Comparative performance analysis of fuzzy PI, PD and PID controllers used in a scalar controlled induction motor drive," in *Proc. Int. Conf. Circuits, Power Comput. Technol. (ICCPCT)*, Mar. 2014, pp. 910–915.
[182] T. Ramesh, A. K. Panda, and S. S. Kumar, "Type-2 fuzzy logic control based MRAS speed estimator for speed sensorless direct torque and flux control of an induction motor drive," *ISA Trans.*, vol. 57, pp. 262–275, Jul. 2015.
[183] S. Padmanaban, Febin Daya J.L., F. Blaabjerg N. Mir-Nasiri, A. H. Ertas, "Numerical implementation of wavelet and fuzzy transform IFOC for three-phase induction motor," *Eng. Sci. Technol. Int. J.*, vol. 19, no. 1, pp. 96–100, Mar. 2016.
[184] J. C. Basilio and S. R. Matos, "Design of PI and PID controllers with transient performance specification," *IEEE Trans. Educ.*, vol. 45, no. 4, pp. 364–370, Nov. 2002.
[185] R. R. Ponce and D. V. Talavera, "FPGA implementation of decimal division for motor control drives," *IEEE Latin Amer. Trans.*, vol. 14, no. 9, pp. 3980–3985, Sep. 2016.

MAHAMMAD A. HANNAN (M'10–SM'17) received the B.Sc. degree in electrical and electronic engineering from the Chittagong University of Engineering and Technology, Chittagong, Bangladesh, in 1990, and the M.Sc. and Ph.D. degrees in electrical, electronic, and systems engineering from the Universiti Kebangsaan Malaysia, Bangi, Malaysia, in 2003 and 2007, respectively. He is currently a Professor of intelligent systems with the Department of Electrical Power Engineering, College of Engineering, Universiti Tenaga Nasional, Malaysia. He has published over 300 papers in the reputed journals and indexed conference proceedings His research interests include intelligent controllers, power electronics, hybrid vehicles, energy storage systems, image and signal processing, and artificial intelligence. He has received a numbers of Gold Awards for his innovative research in ITEX, MTE, INNOFEST, SIIF, and PERINTIS. He is an Associate Editor of the IEEE Access and a Reviewer of many related IEEE Transactions.

JAMAL ABD ALI received the B.Sc. degree in electrical and electronics engineering from the University of Technology, Iraq, in 2005, the M.Sc. degree in power engineering from the College of Electrical and Electronic Engineering Techniques, Iraq, in 2010, and the Ph.D. degree in electrical and electronic engineering from the Department of Electrical, Electronics and Systems Engineering, Universiti Kebangsaan Malaysia, in 2016. He is currently with the South Electrical Station, General Company of Electricity Production Middle Region, Ministry of Electricity, Baghdad, Iraq. His research interests include intelligent controllers for induction motors using optimization methods to enhance performance efficiency.

PIN JERN KER received the B.Eng. degree (Hons.) in electrical and electronic engineering from the Universiti Tenaga Nasional (UNITEN), Malaysia, in 2009, and the Ph.D. degree in electronic and electrical engineering from The University of Sheffield, U.K. He is currently a Senior Lecturer with the Department of Electrical Power Engineering, UNITEN. He is also the Head of the Unit (Electronics & IT) with the Institute of Power Engineering, a research institute of UNITEN. His research interests are the simulation and characterization of photodetectors, optical sensing, and design of monitoring and control system for energy-related applications.

AZAH MOHAMED (M'88–SM'05) received the B.Sc. degree from the University of London in 1978, and the M.Sc. and Ph.D. degrees from Universiti Malaya in 1988 and 1995, respectively. She is currently a Professor with the Department of Electrical, Electronic and Systems Engineering, Universiti Kebangsaan Malaysia. Her main research interests are in power system security, power quality, and artificial intelligence.

MOLLA S. H. LIPU received the B.S. degree in electrical and electronic engineering from the Islamic University of Technology, Gazipur, Bangladesh, in 2008, and the M.S. degree in energy from the Asian Institute of Technology, Bangkok, Thailand, in 2013. He is currently pursuing the Ph.D. degree with the Centre for Integrated Systems Engineering and Advanced Technologies, FKAB, Universiti Kebangsaan Malaysia, Bangi, Malaysia. He is also an Assistant Professor of electrical and electronic engineering with the University of Asia Pacific, Dhaka, Bangladesh. His research interests include energy storage systems, artificial intelligence, model optimization, and hybrid renewable energy system.

AINI HUSSAIN (M'98) received the B.Sc. degree in electrical engineering from Louisiana State University, Baton Rouge, LA, USA, the M.Sc. degree from The University of Manchester Institute of Science and Technology, U.K., and the Ph.D. degree from Universiti Kebangsaan Malaysia. She is currently a Professor with the Centre for Integrated Systems Engineering and Advanced Technologies, Faculty of Engineering and Built Environment, Universiti Kebangsaan Malaysia. Her research interests include decision support systems, machine learning, pattern precognition, and signal and image processing.